SUPPLEMENTARY MATERIAL

for

Frequency modulation reveals the phasing of orbital eccentricity during Cretaceous Oceanic Anoxic Event II and the Eocene hyperthermals

Jiří Laurin
Institute of Geophysics, Academy of Sciences, Praha, Czech Republic

Stephen R. Meyers
University of Wisconsin – Madison, Department of Geoscience, Madison, USA

Simone Galeotti
Department of Pure and Applied Science, University of Urbino "Carlo Bò", 61029 Urbino (PU), Italy

Luca Lanci
Department of Pure and Applied Science, University of Urbino "Carlo Bò", 61029 Urbino (PU), Italy

LIST OF SUPPLEMENTARY MATERIAL ITEMS

Table S1: Parameters of one-dimensional models discussed in this paper.

Model ref. #	Model name	Astronomical forcing	Threshold	Proxy	Sedimentation rate [cm/kyr]	Temporal resolution of forcing	Spatial resolution of output
1	Rand200	-	-	n = (rand*400)-200	constant, 1 cm/kyr	2 kyr	2 cm
2	Rand200sin100	-	-	s+n = 100*sin(2πt/110) + (rand*400)-200	constant, 1 cm/kyr	2 kyr	2 cm
3	ECC const1	Eccentricity (ecc) La2011 52-55 Ma	-	e = ecc	constant, 1 cm/kyr	5 kyr	5 cm
4	ECC NORM-PROP k20	Eccentricity (ecc) La2010d 96-100 Ma	-	e = ecc	S = 0.5 + (ecc x 20)	5 kyr	5 cm
5	ECC INV-PROP k10	Eccentricity (ecc) La2010d 96-100 Ma	-	e = ecc	S = 1.25 - (ecc x 10)	5 kyr	5 cm
6	PRECclip const1 rsp5cm	Prec. Index (pri *) La2010d 93-97 Ma	-	p = exp[(-pri-0.03)/0.015]+0.35	constant, 1 cm/kyr	5 kyr	5 cm
7	PRECclip const1 rsp10 cm	Prec. Index (pri *) La2010d 93-97 Ma	-	p = exp[(-pri-0.03)/0.015]+0.35	constant, 1 cm/kyr	5 kyr	10 cm
8	PRECclip const1 rsp10 cm shifted 5 cm	Prec. Index (pri *) La2010d 93-97 Ma	-	p = exp[(-pri-0.03)/0.015]+0.35	constant, 1 cm/kyr	5 kyr	10 cm, shifted by 5 cm
9	PRECclip const1 rsp13 cm	Prec. Index (pri *) La2010d 93-97 Ma	-	p = exp[(-pri-0.03)/0.015]+0.35	constant, 1 cm/kyr	5 kyr	13 cm
10	PRECclip const1 rsp13 cm shift 5 cm	Prec. Index (pri *) La2010d 93-97 Ma	-	p = exp[(-pri-0.03)/0.015]+0.35	constant, 1 cm/kyr	5 kyr	13 cm, shifted by 5 cm
11	PRECclip PROP 0,61-0,61	Prec. Index (pri *) La2010d 93-97 Ma	-	p = exp[(-pri-0.03)/0.015]+0.35	S = 0.61 + (p x 0.61)	5 kyr	5 cm
12	PRECclip PROP 0,37-1,00	Prec. Index (pri *) La2010d 93-97 Ma	-	p = exp[(-pri-0.03)/0.015]+0.35	S = 0.37 + (p x 1.00)	5 kyr	5 cm
13	PRECclip INV-PROP 1,12-0,20	Prec. Index (pri *) La2010d 93-97 Ma	-	p = exp[(-pri-0.03)/0.015]+0.35	S = 1.12 - (p x 0.2)	5 kyr	5 cm
14	PRECclip INV-PROP 1,48-0,80	Prec. Index (pri *) La2010d 93-97 Ma	-	p = exp[(-pri-0.03)/0.015]+0.35	S = 1.48 - (p x 0.8)	5 kyr	5 cm
15	PRECclip ECC INV-PROP 1,45-0,25 RESAMPLED	Prec. Index (pri *) and Eccentricity (ecc) La2010d 93-97Ma	-	p = {exp[(-pri-0.03)/0.015]+0.35} + (50 x ecc)	S = 1.45 - (p x 0.25) (for p < 5.4) S = 0.1 (for p ≥ 5.4)	5 kyr	5-15 cm uneven, precession-scale maxima in p avoided
16	PRECclip INV-PROP 1,12-0,20 TH 0.8 min 0.3 max 2.5	Prec. Index (pri *) La2010d 93-97 Ma	TH = 0.8	pTH = 0.3 (for p < TH) pTH = 2.5 (for p ≥ TH) p = exp[(-pri-0.03)/0.015]+0.35	S = 1.12 - (pTH x 0.2)	5 kyr	5 cm
17	PRECclip INV-PROP 1,18-0,20 TH 0.8 min 0.1 max 5.0	Prec. Index (pri *) La2010d 93-97 Ma	TH = 0.8	pTH = 0.1 (for p < TH) pTH = 5.0 (for p ≥ TH) p = exp[(-pri-0.03)/0.015]+0.35	S = 1.18 - (pTH x 0.2)	5 kyr	5 cm
18	PRECclip INV-PROP 1,18-0,20 TH 0.8 min 0.1 max 5.0 GRAD proxy	Prec. Index (pri *) La2010d 93-97 Ma	TH = 0.8	p = exp[(-pri-0.03)/0.015]+0.35	S = 1.18 - (pTH x 0.2) pTH = 0.1 (p < TH) pTH = 5.0 (p ≥ TH)	5 kyr	5 cm
19	PRECclip NORM-PROP 0,37-1,00 TH 0.8 min 0.22 max 2.5	Prec. Index (pri *) La2010d 93-97 Ma	TH = 0.8	pTH = 0.22 (for p < TH) pTH = 2.50 (for p ≥ TH) p = exp[(-pri-0.03)/0.015]+0.35	S = 0.37 + (pTH x 1.00)	5 kyr	5 cm
20	PRECclip NORM-PROP 0,37-1,00 TH 0.8 min 0.22 max 2.5 GRAD proxy	Prec. Index (pri *) La2010d 93-97 Ma	TH = 0.8	p = exp[(-pri-0.03)/0.015]+0.35	S = 0.37 + (pTH x 1.00) pTH = 0.22 (p < TH) pTH = 2.50 (p ≥ TH)	5 kyr	5 cm
21	INVclip0.02 CONST	Eccentricity (ecc) La2010d 93-97 Ma	TH = 0.02	ep = TH (for ecc ≥ TH) ep = ecc (for ecc < TH)	constant, 1 cm/kyr	5 kyr	5 cm
22	INVclip0.03 CONST	Eccentricity (ecc) La2010d 93-97 Ma	TH = 0.03	ep = TH (for ecc ≥ TH) ep = ecc (for ecc < TH)	constant, 1 cm/kyr	5 kyr	5 cm

23	INVclip0.02 NORM-PROP	Eccentricity (ecc) La2010d 93-97 Ma	TH = 0.02	ep = TH (for ecc ≥ TH) ep = ecc (for ecc < TH)	S = 0.65 + (20 x TH) (for ecc ≥ TH) S = 0.65 + (20 x ecc) (for ecc < TH)	5 kyr	5 cm
24	INVclip0.03 NORM-PROP	Eccentricity (ecc) La2010d 93-97 Ma	TH = 0.03	ep = TH (for ecc ≥ TH) ep = ecc (for ecc < TH)	S = 0.55 + (20 x TH) (for ecc ≥ TH) S = 0.55 + (20 x ecc) (for ecc < TH)	5 kyr	5 cm
25	INVclip0.02 INV-PROP	Eccentricity (ecc) La2010d 93-97 Ma	TH = 0.02	ep = TH (for ecc ≥ TH) ep = ecc (for ecc < TH)	S = 1.43 – (25 x TH) (for ecc ≥ TH) S = 1.43 – (25 x ecc) (for ecc < TH)	5 kyr	5 cm
26	INVclip0.03 INV-PROP	Eccentricity (ecc) La2010d 93-97 Ma	TH = 0.03	ep = TH (for ecc ≥ TH) ep = ecc (for ecc < TH)	S = 1.44 – (20 x TH) (for ecc ≥ TH) S = 1.44 – (20 x ecc) (for ecc < TH)	5 kyr	5 cm

**) pri = e sin ω, where ω is longitude of the perihelion*

Table S2: Parameters of two-dimensional models discussed in this paper.

Model ref. #	Model name	Astronomical forcing	Sea level curve	Multiplier a	Multiplier b	Temporal resolution of forcing	Spatial resolution of output
27	MILex highECC 150-200	Eccentricity (ecc) La2010d 94-97 Ma	SL = (e x a) + (e1 x b)	-150	-200	2 kyr	2 cm
28	MILex highECC 150-300	Eccentricity (ecc) La2010d 94-97 Ma	SL = (e x a) + (e1 x b)	-150	-300	2 kyr	2 cm
29	MILex highECC 150-400	Eccentricity (ecc) La2010d 94-97 Ma	SL = (e x a) + (e1 x b)	-150	-400	2 kyr	2 cm
30	MILex lowECC 150-200	Eccentricity (ecc) La2010d 94-97 Ma	SL = (e x a) + (e1 x b)	+150	+200	2 kyr	2 cm
31	MILex lowECC 150-300	Eccentricity (ecc) La2010d 94-97 Ma	SL = (e x a) + (e1 x b)	+150	+300	2 kyr	2 cm
32	MILex lowECC 150-400	Eccentricity (ecc) La2010d 94-97 Ma	SL = (e x a) + (e1 x b)	+150	+400	2 kyr	2 cm

MODEL: SEDIMENTATION-RATE CHANGE

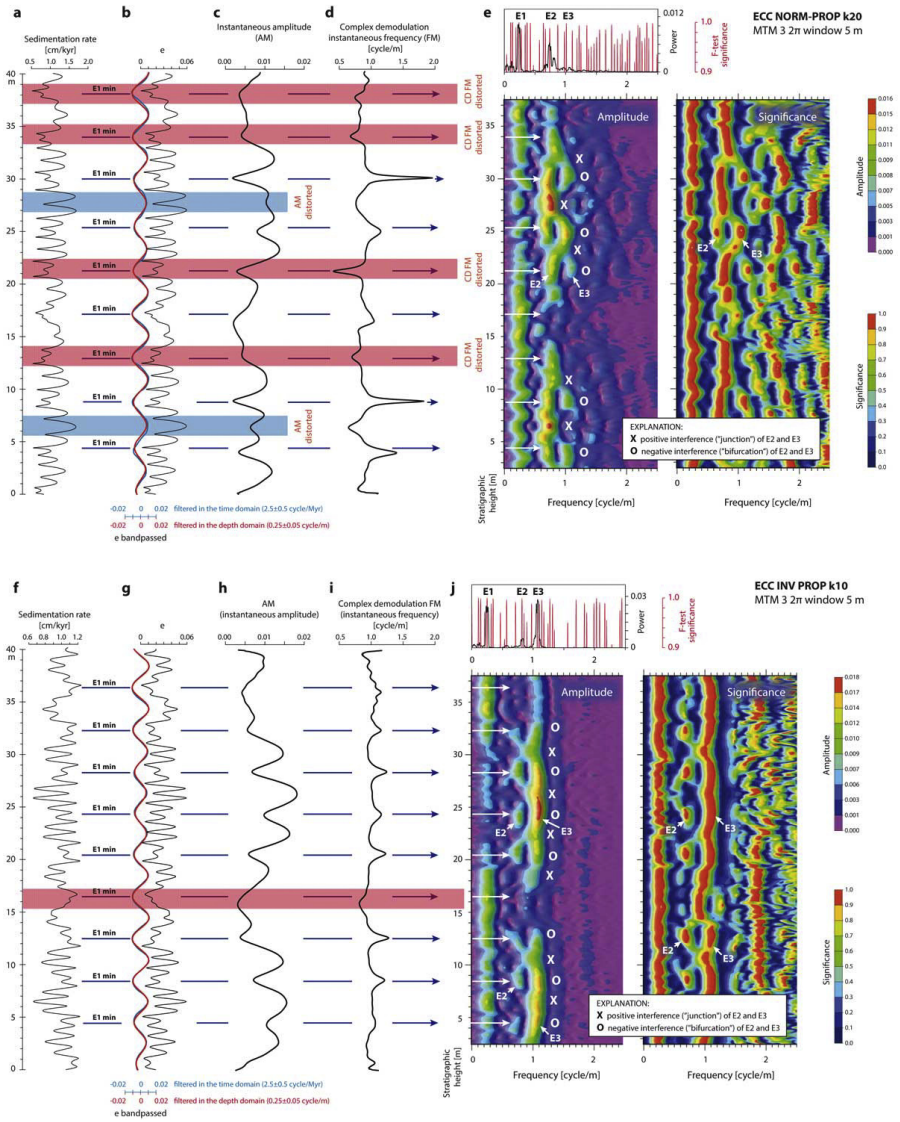

Figure S1.1. Models of eccentricity-paced sedimentation illustrating the preservation and distortion of AM and FM upon sedimentation-rate changes (**models #4 and #5**; Tab. S1). Sedimentation rate was modeled as **(a)** normally and **(f)** reversely proportional to eccentricity (solution La2010d, interval 96-100 Ma). **(b, g)** Orbital eccentricity (e) plotted against stratigraphic height. The model time step is 5 kyr. Bandpassed 405-kyr eccentricity indicated in red and blue. E1min = 405-kyr minimum. Instantaneous amplitude (AM) of the E2+E3 signal in e **(c, h)**, and instantaneous frequency (FM) of the E2+E3 signal in e **(d, i)** were obtained with complex demodulation (CD) using a Taner window, 9.5±2.5 cycle/Myr, and a roll-off rate of 10^4. Stratigraphic height was converted to time using average sedimentation rate of 10.17468 m/Myr for model ECC NORM PROP k20 (#4) and 9.748463 m/Myr for model ECC INV PROP k10 (#5) and. Both AM

and FM from complex demodulation are sensitive to the selection of filter parameters, and do not provide a robust basis for the interpretation of 405-kyr maxima and minima. **(e, j)** Spectral estimates for the parameter e in the depth domain: MTM (3 2π) power spectral and significance estimates for the entire series (top), and EHA (MTM 3 2π) amplitude and significance obtained with a 5-m moving window. Eccentricity terms E1, E2 and E3 are indicated. Note that well-developed junctions (X) and bifurcations (O) originating from the interference of E2 and E3 provide a feedback to the interpretation of instantaneous frequencies and amplitudes allowing to distinguish pristine modulation patterns from depositional artifacts.

MODEL: UNDERSAMPLING + CLIPPED FORCING

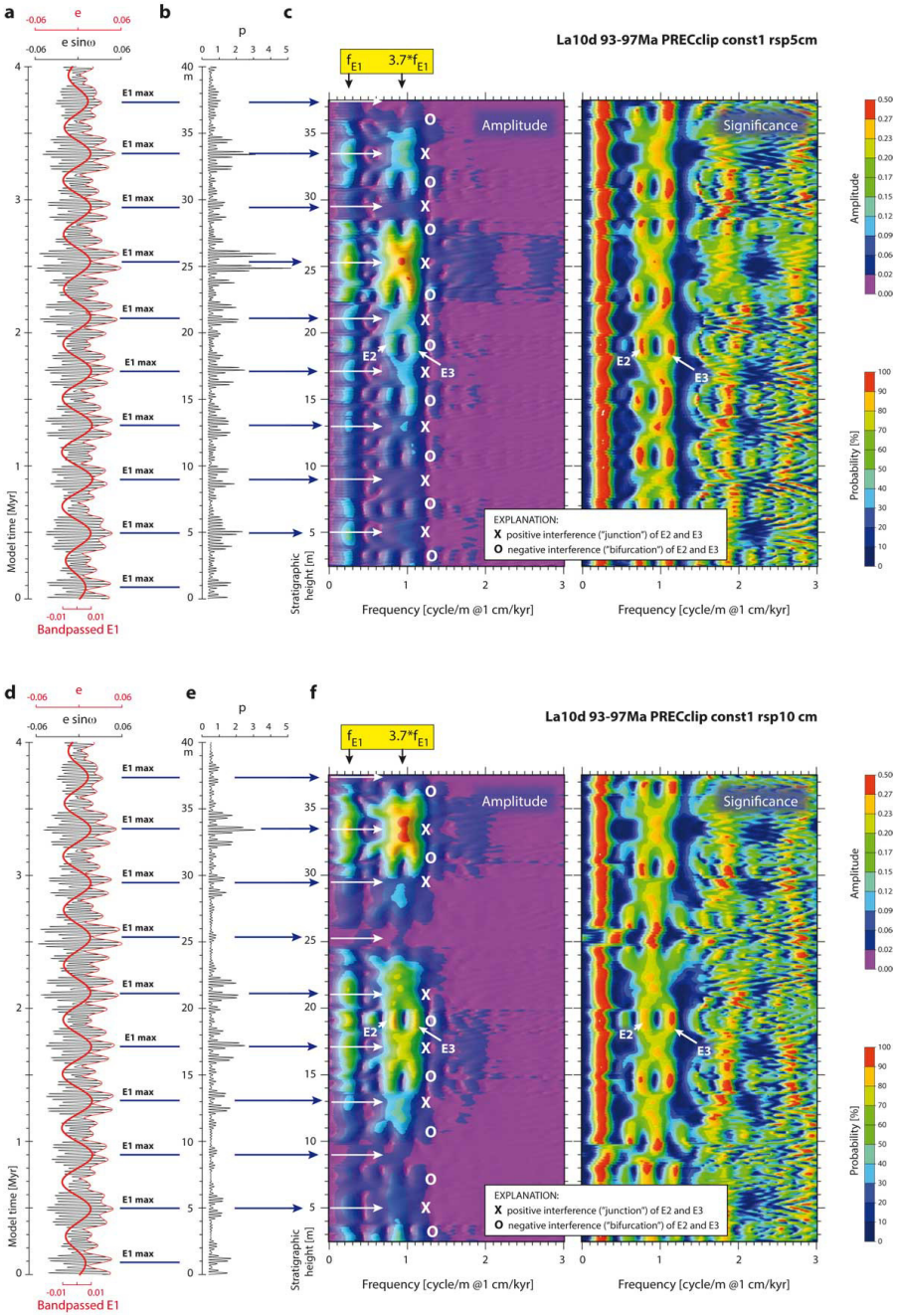

Figure S1.2 (part 1)

MODEL: UNDERSAMPLING + CLIPPED FORCING

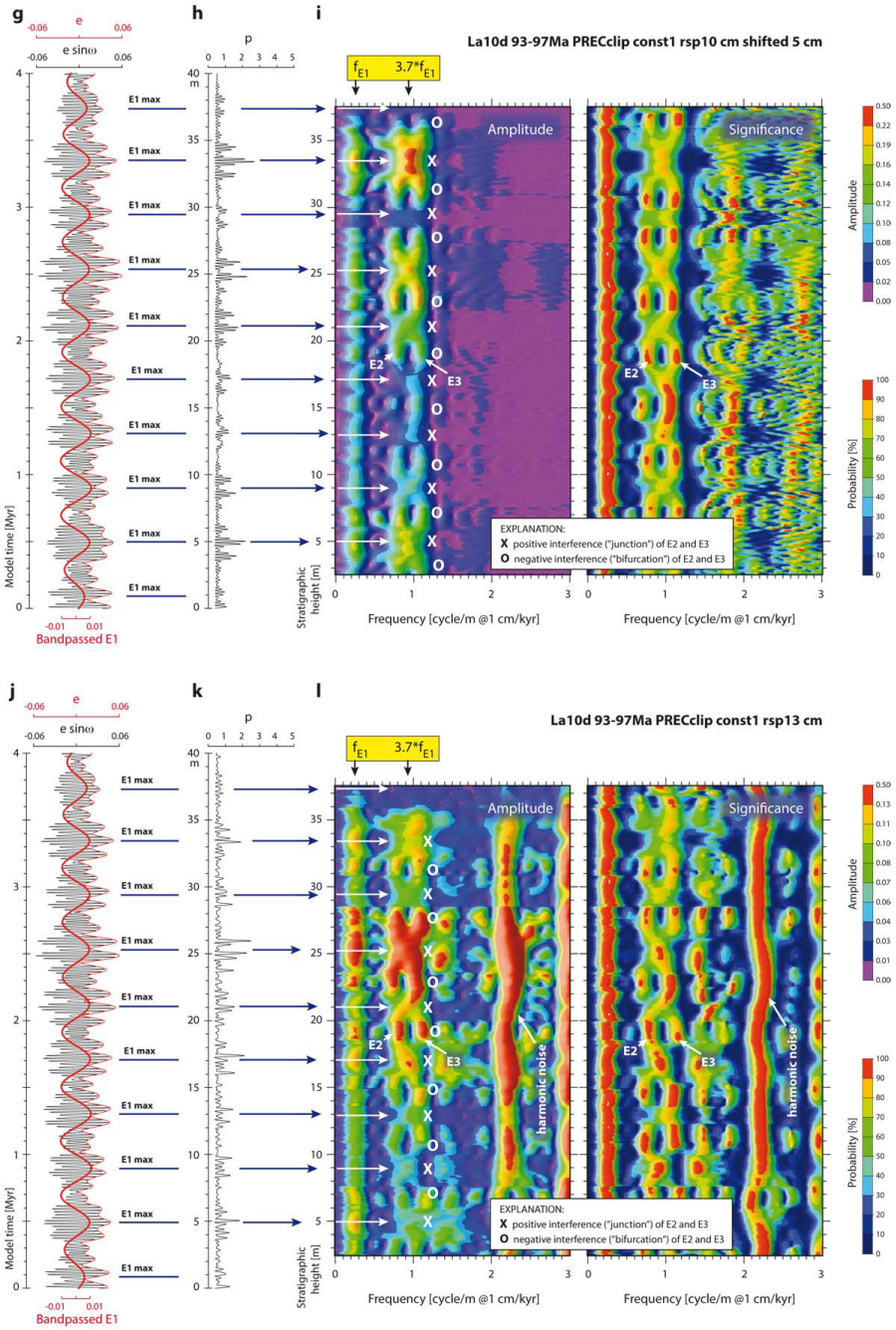

Figure S1.2 (part 2)

MODEL: UNDERSAMPLING + CLIPPED FORCING

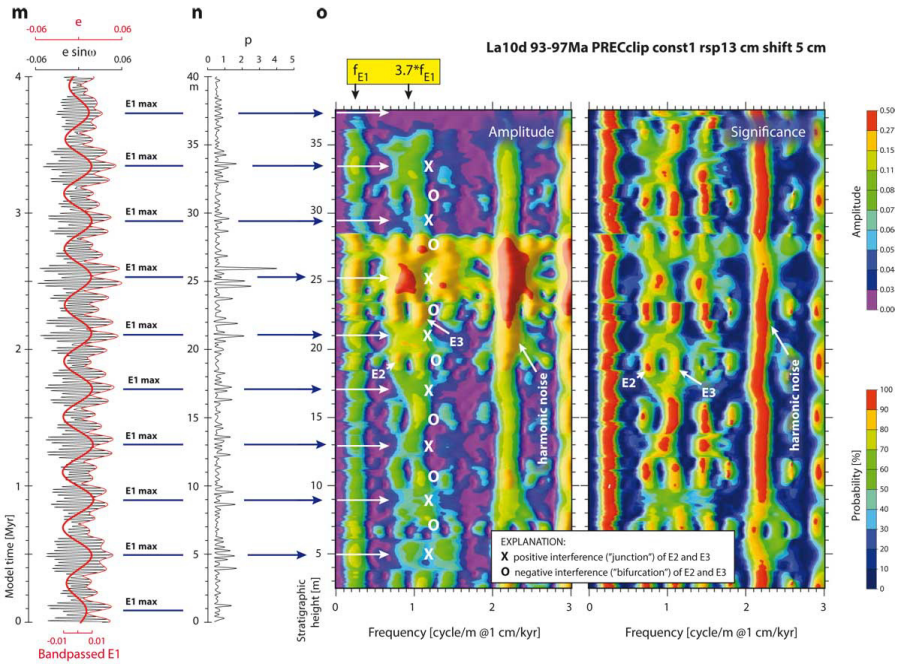

Figure S1.2. A simple model of precession-paced sedimentation assuming constant sedimentation rate and a linear response of lithological/geochemical proxy (p) to a clipped precessional index. Five model runs shown here explore the influence of undersampling on the record of frequency modulation. **Models #6 through #10** (Tab. S1). **(a, d, g, j, m)** Model input; La2010d (93-97 Ma) solution for eccentricity (e) and precessional index (e sin ω, where ω is longitude of the perihelion) plotted against time. **(b)** A proxy of precession-driven insolation (p) plotted against stratigraphic height; this proxy is modeled as proportional to a clipped precessional index. The model time step is 5 kyr and sample resolution is 5 cm. **(e)** Same as b, sampled every 10 cm. **(h)** Same as b, sampled every 10 cm, with the first sample taken at the 5 cm height. **(k)** Same as b, sampled every 13 cm. **(n)** Same as b, sampled every 13 cm, with the first sample taken at the 5 cm height. **(c, f, i, l, o)** EHA (MTM 3 2π, 5-m window) amplitude and significance for the proxy parameters shown in b, e, h, k and n. Note that intervals of positive interference of the E2 and E3 signals trace closely the maxima and minima, respectively, in the E1 cycle. Note also that amplitude modulation of the precessional signal in p is very sensitive to sampling strategy. Frequency modulation traced in the EHA spectrograms remains relatively stable and can be used as a feedback on the interpretation of the origin of amplitude modulation. One of the effects of undersampling is the development of a strong harmonic noise at c. 2.2 cycle/m frequency.

MODEL: SEDIMENTATION-RATE CHANGE

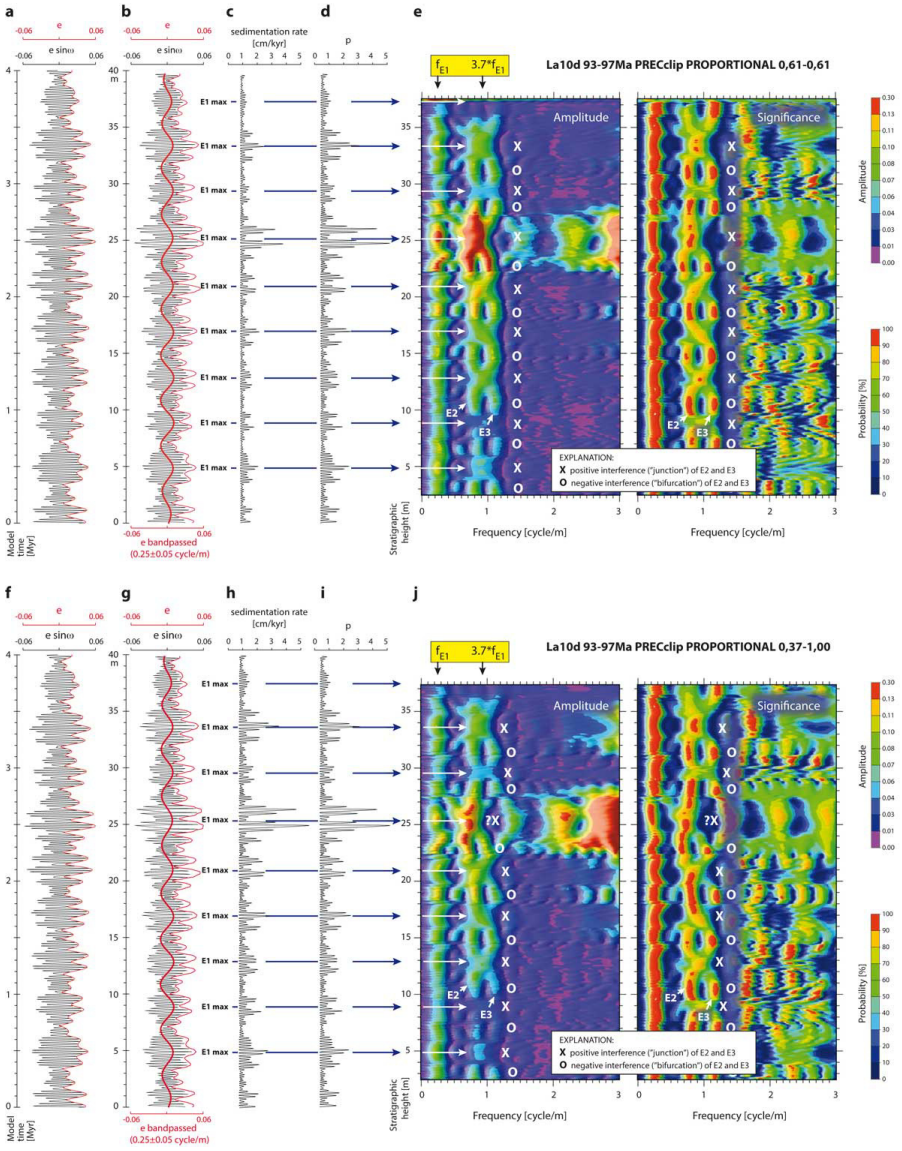

Figure S1.3. A simple model of precession-paced sedimentation assuming a linear response of both sedimentation rate and lithological/geochemical proxy (p) to a clipped precessional index. **Models #11 and #12** (Tab. S1). **(a, f)** Model input; La2010d (93-97 Ma) solution for eccentricity (e) and precessional index (e sin ω, where ω is longitude of the perihelion) plotted against time. **(b, g)** Model input plotted against stratigraphic height. **(c, h)** Sedimentation rate modeled as a linear response to clipped precessional index. **(d, i)** A proxy of precession-driven insolation (p) plotted against stratigraphic height; this proxy is modeled as proportional to a clipped precessional index. The model time step, i.e., the maximum temporal resolution of the modeled stratigraphy, is 5 kyr. **(e, j)** EHA (MTM 3 2π, 5-m window) amplitude and significance for the proxy parameter

shown in d and i; intervals of positive interference of the E2 and E3 signals are marked with X ("junctions") and intervals of negative interference are indicated by O ("bifurcations"). Note that these interference patters trace closely the maxima and minima, respectively, in the E1 cycle. The junctions appear generally more stable, centered within a few tens of kyr of the E1 maxima.

MODEL: SEDIMENTATION-RATE CHANGE

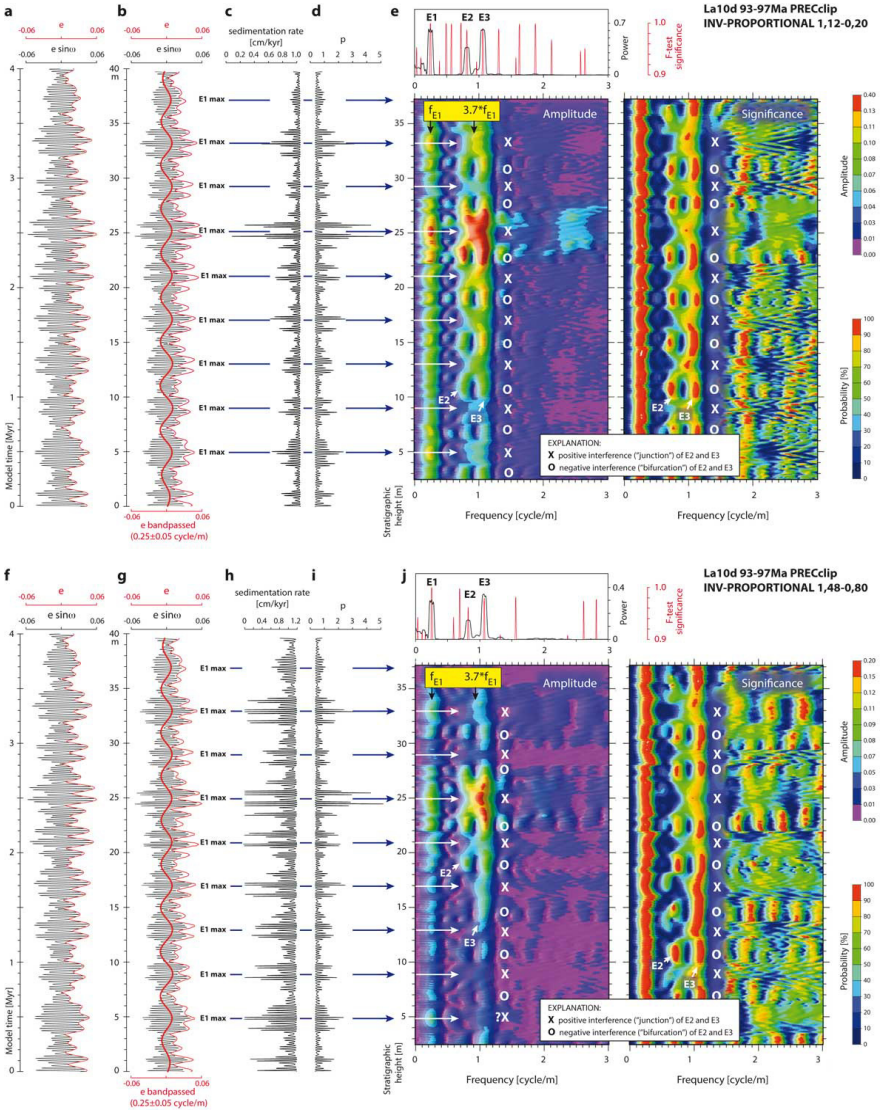

Figure S1.4. A simple model of precession-paced sedimentation assuming a linear, reversely proportional response of sedimentation rate to a clipped precessional index. **Models #13 and #14** (Tab. S1). **(a, f)** Model input; La2010d (93-97 Ma) solution for eccentricity (e) and precessional index (e sin ω, where ω is longitude of the perihelion) plotted against time. **(b, g)** Model input plotted against stratigraphic height. **(c, h)** Sedimentation rate modeled as a linear, reverse response to clipped precessional index. **(d, i)** A proxy of precession-driven insolation (p) plotted against stratigraphic height; this proxy is modeled as normally proportional to a clipped precessional index. The model time step, i.e., the maximum temporal resolution of the modeled stratigraphy, is 5 kyr. **(e, j)** Spectral estimates for the parameter p: MTM (3 2π) power spectral and significance estimates for the entire series (top), and EHA (MTM 3 2π) amplitude and significance obtained with a 5-m moving window. Eccentricity terms E1, E2 and E3 are indicated. Intervals of positive interference of the E2 and E3 signals are marked with X ("junctions") and intervals of negative interference are indicated by O ("bifurcations"). Note that these interference patters trace closely the maxima and minima, respectively, in the E1 cycle.

MODEL: SEDIMENTATION RATE + UNDERSAMPLING

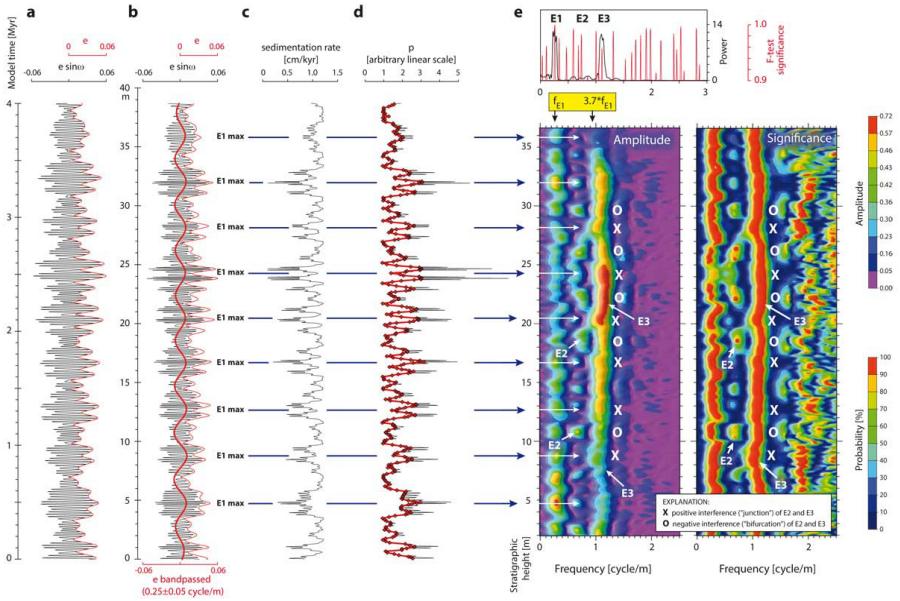

Figure S1.5. A model of precession- and eccentricity-paced sedimentation designed to examine the effect of sedimentation-rate changes and undersampling that systematically avoids one phase of the precessional signal (similar to the avoidance of black shales and cherts in the IRM record from Furlo; Lanci et al. 2010). **Model #15** (Tab. S1). **(a)** Model input; La2010d solution for eccentricity (e) and precessional index (e sin ω, where ω is longitude of the perihelion), interval 93-97 Ma, plotted against time. **(b)** Model input plotted against stratigraphic height. Bandpassed 405-kyr (E1) signal is shown in red. **(c)** Sedimentation rate plotted against stratigraphic height; it is modeled as reversely proportional to the precessional index (clipped at 0) and orbital eccentricity. The eccentricity component is applied as an imposed cycle (see Table S1 for details). **(d)** Proxy parameter (p) modeled as proportional to the precessional index (clipped at 0) and orbital eccentricity (imposed). The original series (thin black curve) has a temporal resolution of 5 kyr. It was resampled unevenly, every 5-15 cm, at precession-scale minima in the proxy parameter (red line and diamonds). This sampling strategy is supposed to mimic the IRM sampling at Furlo, which focused on limestone lithologies while avoiding black shales and cherts (cf. Lanci et al. 2010). **(e)** Spectral estimates for the parameter p: MTM (3 2π) power spectral and significance estimates for the entire series (top), and EHA (MTM 3 2π) amplitude and significance obtained with a 4-m moving window. Eccentricity terms E1, E2 and E3 are indicated. Intervals of positive interference of the E2 and E3 signals are marked with X ("junctions") and intervals of negative interference are indicated by O ("bifurcations"). In spite of a severe distortion due to sedimentation-rate changes and undersampling the interference patters trace maxima and minima in the E1 cycle in most of the study interval.

Note on the comparison with Furlo OAE II results (Fig. 6):
This model exhibits a relatively strong distortion of the E2-E3 interference, with most of the variance shifted towards the E3 signal. This distortion is attributable to a strong sedimentation-rate variability used in the model. The IRM data from Furlo exhibit interference that is closer to the original modulation of eccentricity forcing (cf. Fig. 1) suggesting that the astronomical-scale variability in sedimentation rate is less pronounced in the Furlo section as compared to this model.

MODEL: SEDIMENTATION RATE + STRONG THRESHOLD

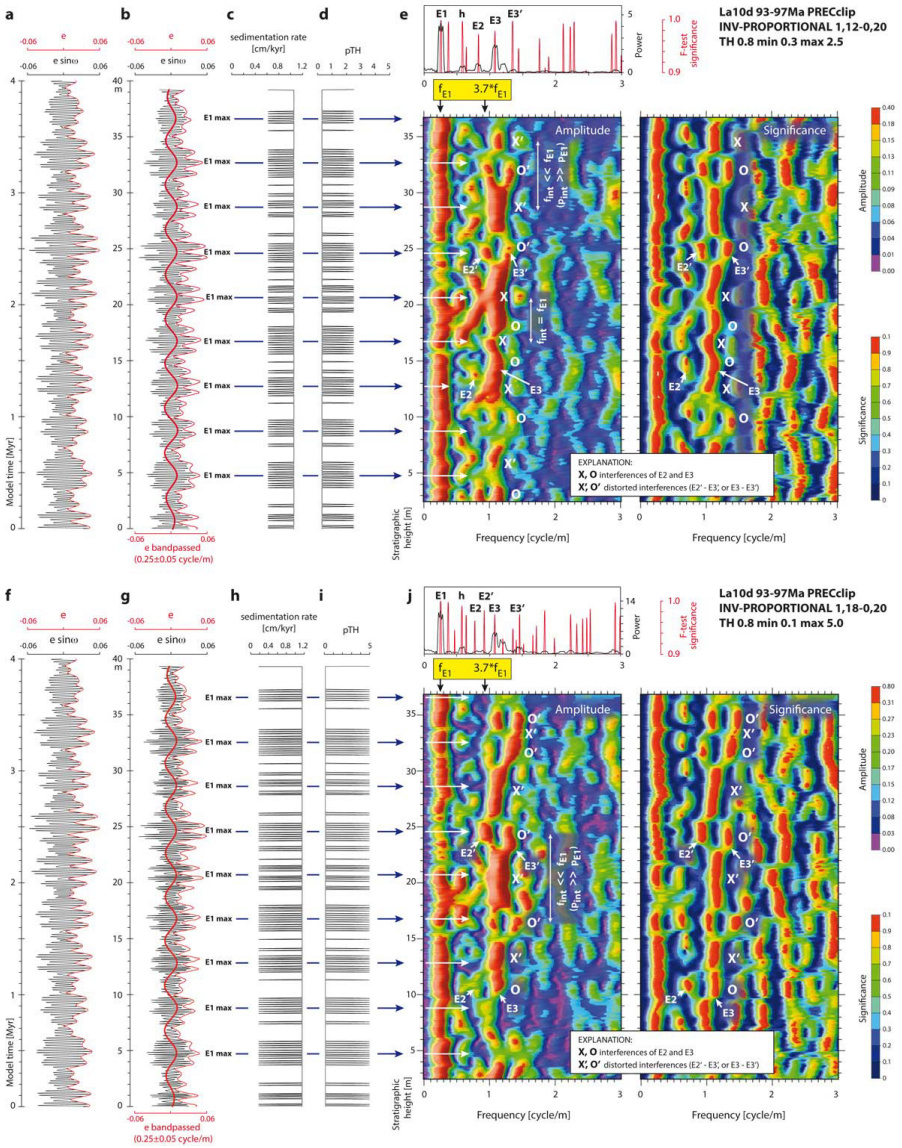

Figure S1.6 (part 1)

MODEL: SEDIMENTATION RATE + STRONG THRESHOLD

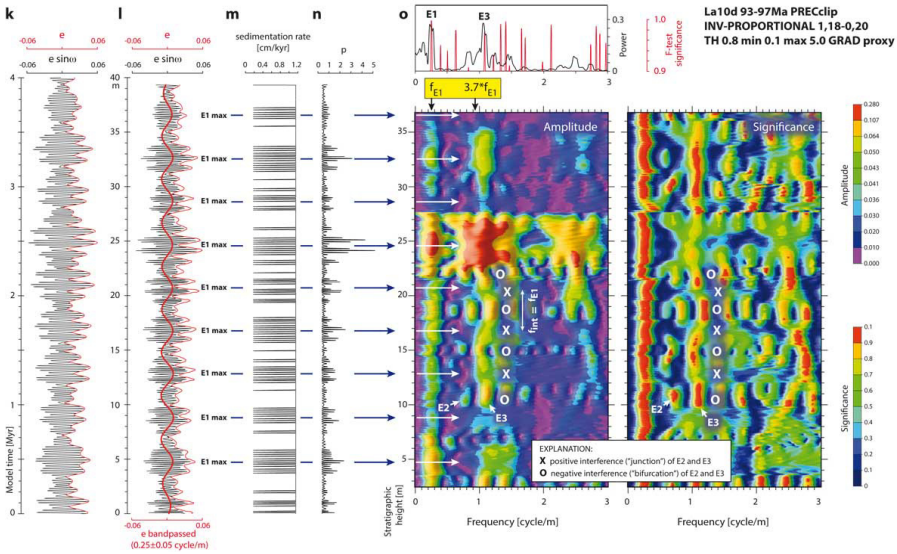

Figure S1.6. A simple model of precession-paced sedimentation assuming a non-linear, reverse response of sedimentation rate to a clipped precessional index. **Models #16 through #18** (Tab. S1). **(a, f, k)** Model input; La2010d (93-97 Ma) solution for eccentricity (e) and precessional index (e sin ω, where ω is longitude of the perihelion) plotted against time. **(b, g, l)** Model input plotted against stratigraphic height. **(c, h, m)** Sedimentation rate modeled as a reverse, threshold response to clipped precessional index. **(d, i)** A proxy of precession-driven insolation (pTH) plotted against stratigraphic height; this proxy is modeled as a threshold response to clipped precessional index. The model time step, i.e., the maximum temporal resolution of the modeled stratigraphy, is 5 kyr. **(n)** Same as d and i, modeled as a linear response to clipped precessional index**. (e, j, o)** Spectral estimates for the parameters pTH and p: MTM (3 2π) power spectral and significance estimates for the entire series (top), and EHA (MTM 3 2π) amplitude and significance obtained with a 5-m moving window. Eccentricity terms E1, E2 and E3 are indicated. E2' and E3' refer to distorted ("blue shifted") frequencies of E2 and E3. Harmonic noise is labeled "h". In these models, interference patters are often strongly distorted, and do not trace the maxima and minima in the E1 cycle. The distorted patterns (labeled X' and O') are, however, readily distinguishable from pristine modulation by the lack of E1-like rhythm ($f_{int} < f_{E1}$) and apparent "blue shift" of the interfering frequencies.

MODEL: SEDIMENTATION RATE + STRONG THRESHOLD

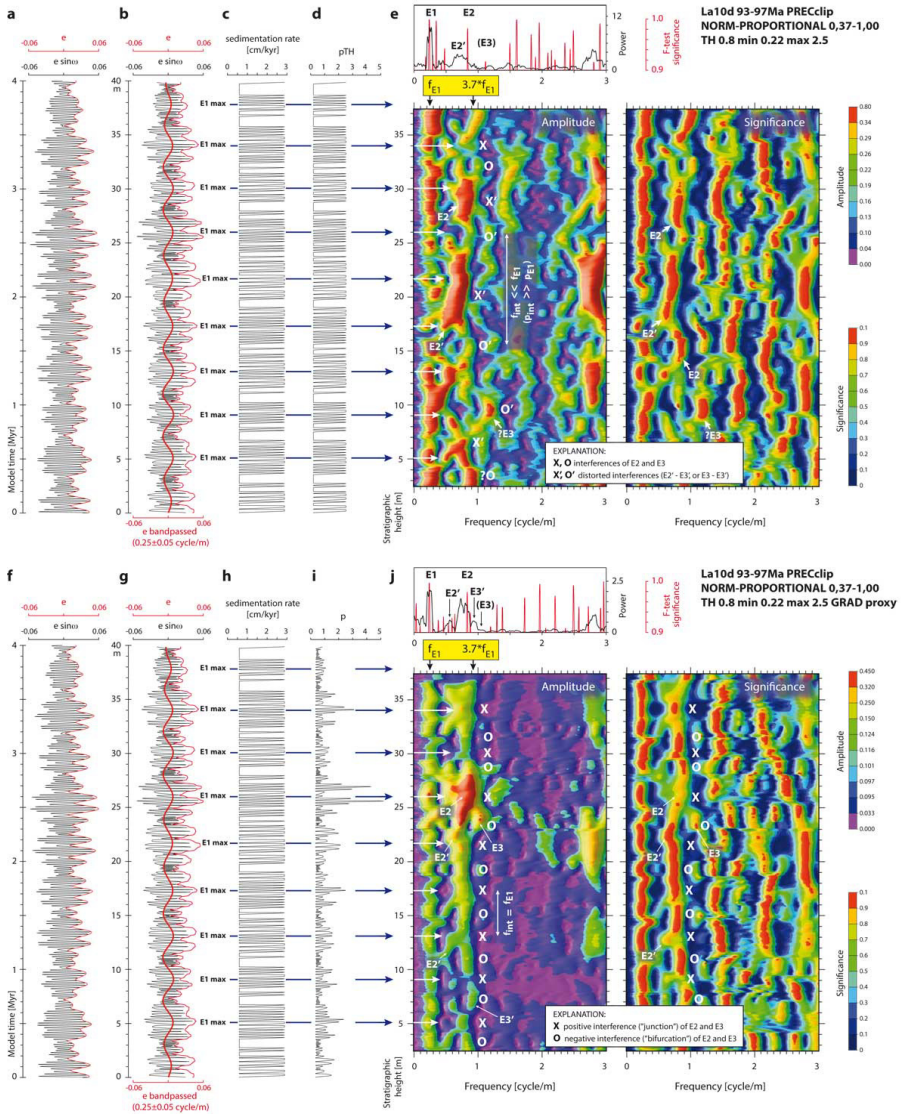

Figure S1.7. A simple model of precession-paced sedimentation assuming a non-linear response of sedimentation rate to a clipped precessional index. **Models #19 and #20** (Tab. S1). **(a, f)** Model input; La2010d (93-97 Ma) solution for eccentricity (e) and precessional index (e sin ω, where ω is longitude of the perihelion) plotted against time. **(b, g)** Model input plotted against stratigraphic height. **(c, h)** Sedimentation rate modeled as a threshold response to clipped precessional index. **(d)** A proxy of precession-driven insolation (pTH) plotted against stratigraphic height; this proxy is modeled as a threshold response to clipped precessional index. The model time step, i.e., the maximum temporal resolution of the modeled stratigraphy, is 5 kyr. **(i)** Same as d, modeled as a linear, normally proportional response to clipped precessional index**. (e, j)** Spectral estimates for the parameters pTH and p: MTM (3 2π) power spectral and significance estimates for the entire series (top), and EHA (MTM 3 2π) amplitude and

significance obtained with a 5-m moving window. Eccentricity terms E1, E2 and E3 are indicated. E2' and E3' refer to distorted ("red shifted") frequencies of E2 and E3. In these models, interference patters are strongly distorted, and in many cases do not trace the maxima and minima in the E1 cycle. The distorted patterns are, however, readily distinguishable from pristine modulation by the lack of E1-like rhythm and apparent "red shift" of the interfering frequencies.

MODEL: SEDIMENTATION RATE + REVERSE CLIP

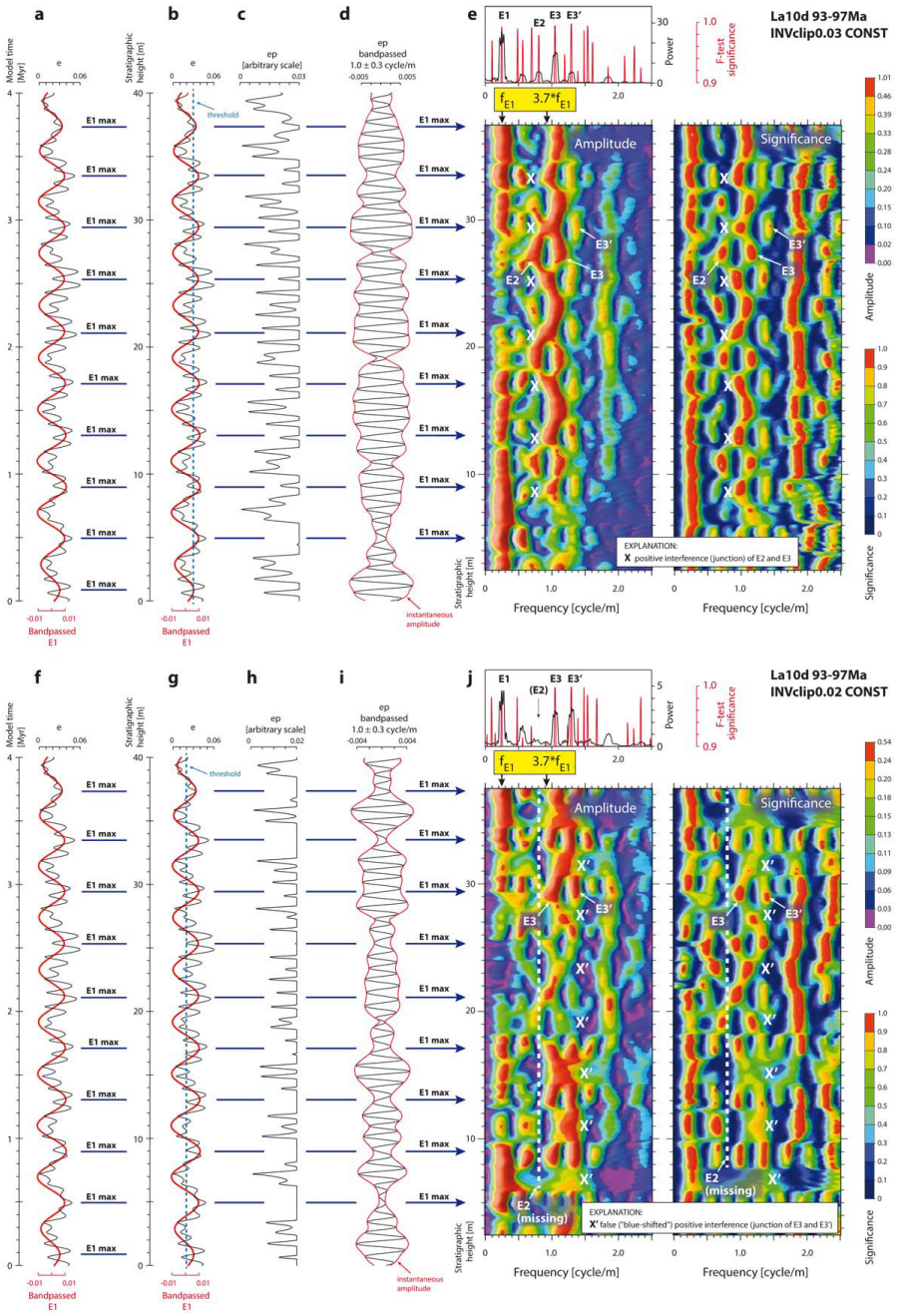

Figure S1.8. A simple model of eccentricity-paced sedimentation assuming a constant sedimentation rate and a non-linear (reversely clipped) response of sedimentary proxy (ep) to orbital eccentricity (e). **Models #21 and #22** (Tab. S1). **(a, f)** Model input; La2010d solution for eccentricity, interval 93-97 Ma, plotted against time. **(b, g)** Model input plotted against stratigraphic height. **(c, h)** A non-linear proxy of orbital

eccentricity plotted against stratigraphic height. This proxy is modeled as proportional to orbital eccentricity, but only for eccentricity values below 0.03 (c) and 0.02 (h), i.e., the proxy is considered insensitive to eccentricity maxima. The model time step is 5 kyr. **(d, i)** Parameter ep filtered in the E2-E3 band (1.0±0.3 Gaussian filter). Note that AM of the E2-E3 signal is strongly distorted, and does not trace the maxima and minima in 405-kyr (E1) eccentricity. **(e, j)** Spectral estimates for the parameter ep: MTM (3 2π) power spectral and significance estimates for the entire series (top), and EHA (MTM 3 2π) amplitude and significance obtained with a 5-m moving window. Eccentricity terms E1, E2 and E3 are indicated. E3' refers to a distorted ("blue shifted") frequency of E3. Intervals of positive interference of the E2 and E3 signals are marked with X ("junctions"). These interference patters trace closely the maxima in the E1 cycle (E1 max). With an increasing distortion, however, the E2 signal fades and the variance is transferred towards a new spectral maximum E3'. This change gives rise to new, "blue-shifted" interference patterns (X') that are out-of-phase from E1 maxima. The "blue shift" can serve as a diagnostic feature distinguishing pristine modulation from artifacts.

MODEL: SEDIMENTATION RATE + REVERSE CLIP

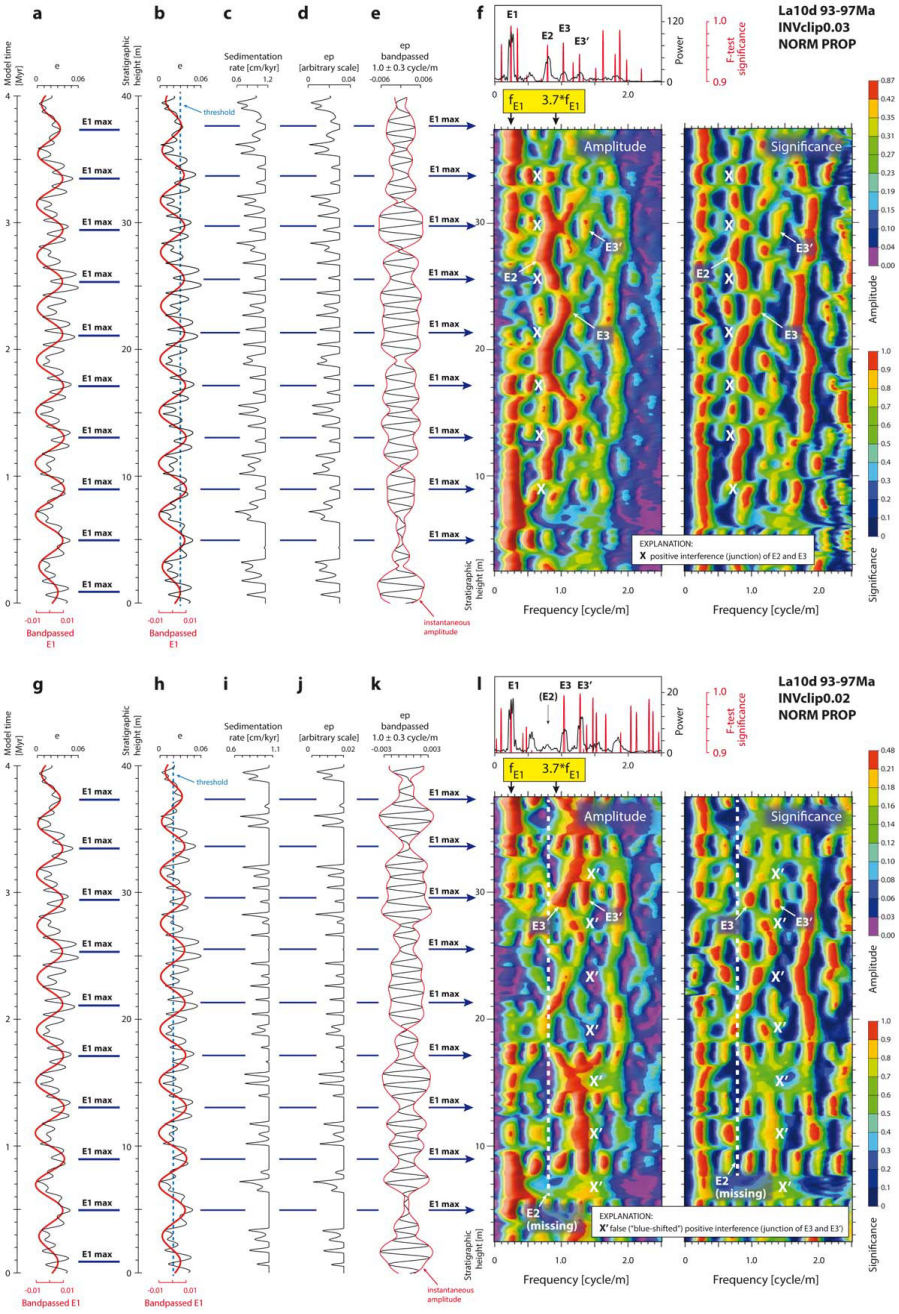

Figure S1.9. A simple model of eccentricity-paced sedimentation assuming a non-linear (reversely clipped) response of both sedimentation rate and sedimentary proxy (ep) to orbital eccentricity (e). **Models #23 and #24** (Tab. S1). **(a, g)** Model input; La2010d solution for eccentricity, interval 93-97 Ma, plotted against time. **(b, h)** Model input

plotted against stratigraphic height. **(c, i)** Sedimentation rate plotted against stratigraphic height; it is modeled as proportional to orbital eccentricity, but only for eccentricity values below 0.03 (c) and 0.02 (i), i.e., the sedimentation rate is considered insensitive to eccentricity maxima. **(d, j)** A non-linear proxy of orbital eccentricity plotted against stratigraphic height. This proxy is modeled as proportional to orbital eccentricity, but only for eccentricity values below 0.03 (d) and 0.02 (j), i.e., the proxy is considered insensitive to eccentricity maxima. The model time step is 5 kyr. **(e, k)** Parameter ep filtered in the E2-E3 band (1.0±0.3 Gaussian filter). Note that AM of the E2-E3 signal is strongly distorted, and does not trace the maxima and minima in 405-kyr (E1) eccentricity. **(f, l)** Spectral estimates for the parameter ep: MTM (3 2π) power spectral and significance estimates for the entire series (top), and EHA (MTM 3 2π) amplitude and significance obtained with a 5-m moving window. Eccentricity terms E1, E2 and E3 are indicated. E3' refers to a distorted ("blue shifted") frequency of E3. Intervals of positive interference of the E2 and E3 signals are marked with X ("junctions"). These interference patters trace closely the maxima in the E1 cycle (E1 max). With an increasing distortion, however, the E2 signal fades and the variance is transferred towards a new spectral maximum E3'. This change gives rise to new, "blue-shifted" interference patterns (X') that are out-of-phase from E1 maxima. The "blue shift" can serve as a diagnostic feature distinguishing pristine modulation from artifacts.

MODEL: SEDIMENTATION RATE + REVERSE CLIP

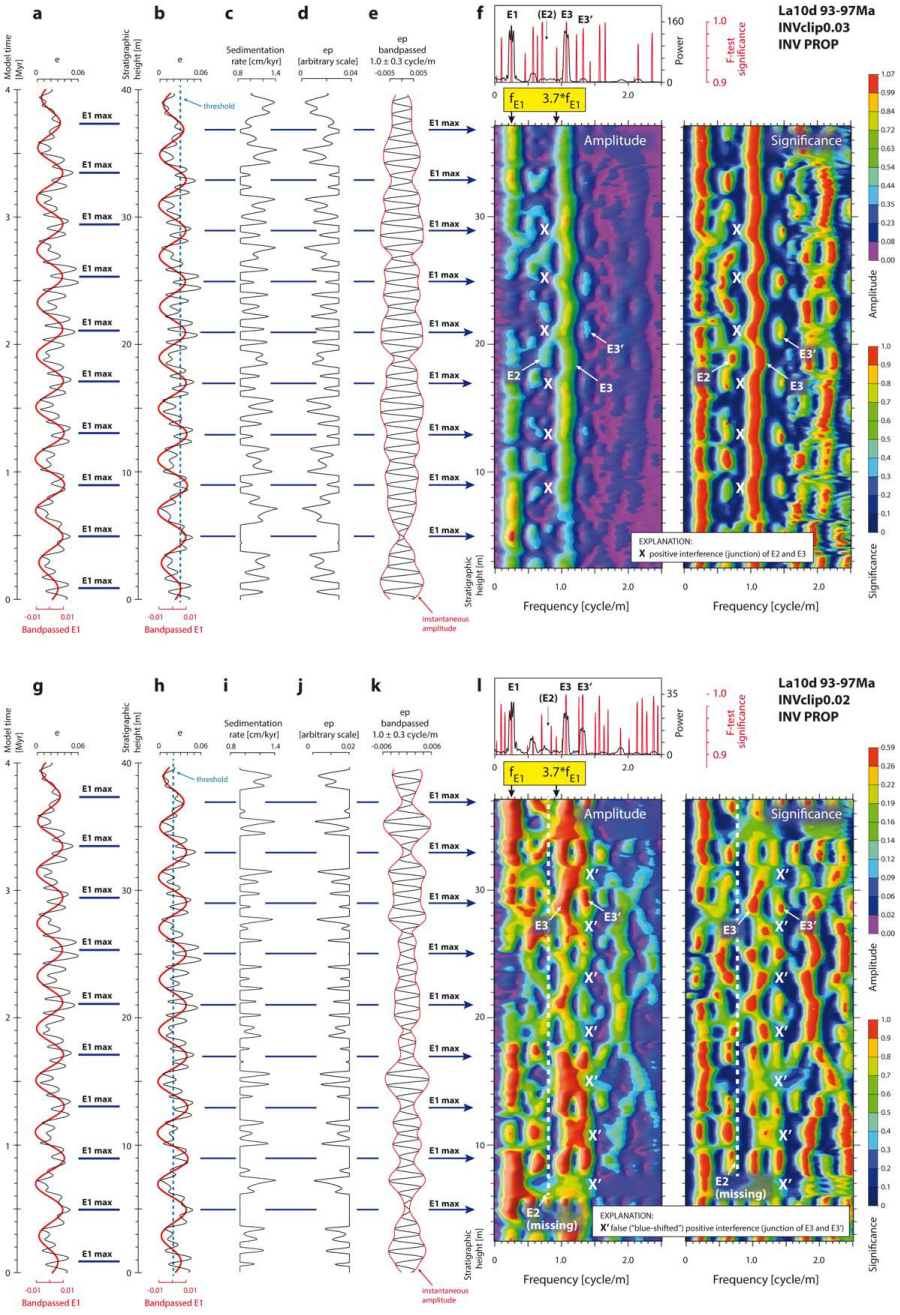

Figure S1.10. A simple model of eccentricity-paced sedimentation assuming a non-linear (reversely clipped) response of both sedimentation rate and sedimentary proxy (ep) to orbital eccentricity (e). **Models #25 and #26** (Tab. S1). **(a, g)** Model input; La2010d solution for eccentricity, interval 93-97 Ma, plotted against time. **(b, h)** Model

input plotted against stratigraphic height. **(c, i)** Sedimentation rate plotted against stratigraphic height; it is modeled as reversely proportional to orbital eccentricity, but only for eccentricity values below 0.03 (c) and 0.02 (i), i.e., the sedimentation rate is considered insensitive to eccentricity maxima. **(d, j)** A non-linear proxy of orbital eccentricity plotted against stratigraphic height. This proxy is modeled as reversely proportional to orbital eccentricity, but only for eccentricity values below 0.03 (d) and 0.02 (j), i.e., the proxy is considered insensitive to eccentricity maxima. The model time step is 5 kyr. **(e, k)** Parameter ep filtered in the E2-E3 band (1.0±0.3 Gaussian filter). Note that AM of the E2-E3 signal is strongly distorted, and does not trace the maxima and minima in 405-kyr (E1) eccentricity. **(f, l)** Spectral estimates for the parameter ep: MTM (3 2π) power spectral and significance estimates for the entire series (top), and EHA (MTM 3 2π) amplitude and significance obtained with a 5-m moving window. Eccentricity terms E1, E2 and E3 are indicated. E3' refers to a distorted ("blue shifted") frequency of E3. Intervals of positive interference of the E2 and E3 signals are marked with X ("junctions"). These interference patters trace closely the maxima in the E1 cycle (E1 max). With an increasing distortion, however, the E2 signal fades and the variance is transferred towards a new spectral maximum E3'. This change gives rise to new, "blue-shifted" interference patterns (X') that are out-of-phase from E1 maxima. The "blue shift" can serve as a diagnostic feature distinguishing pristine modulation from artifacts.

MODEL: TWO-DIMENSIONAL CONTROL

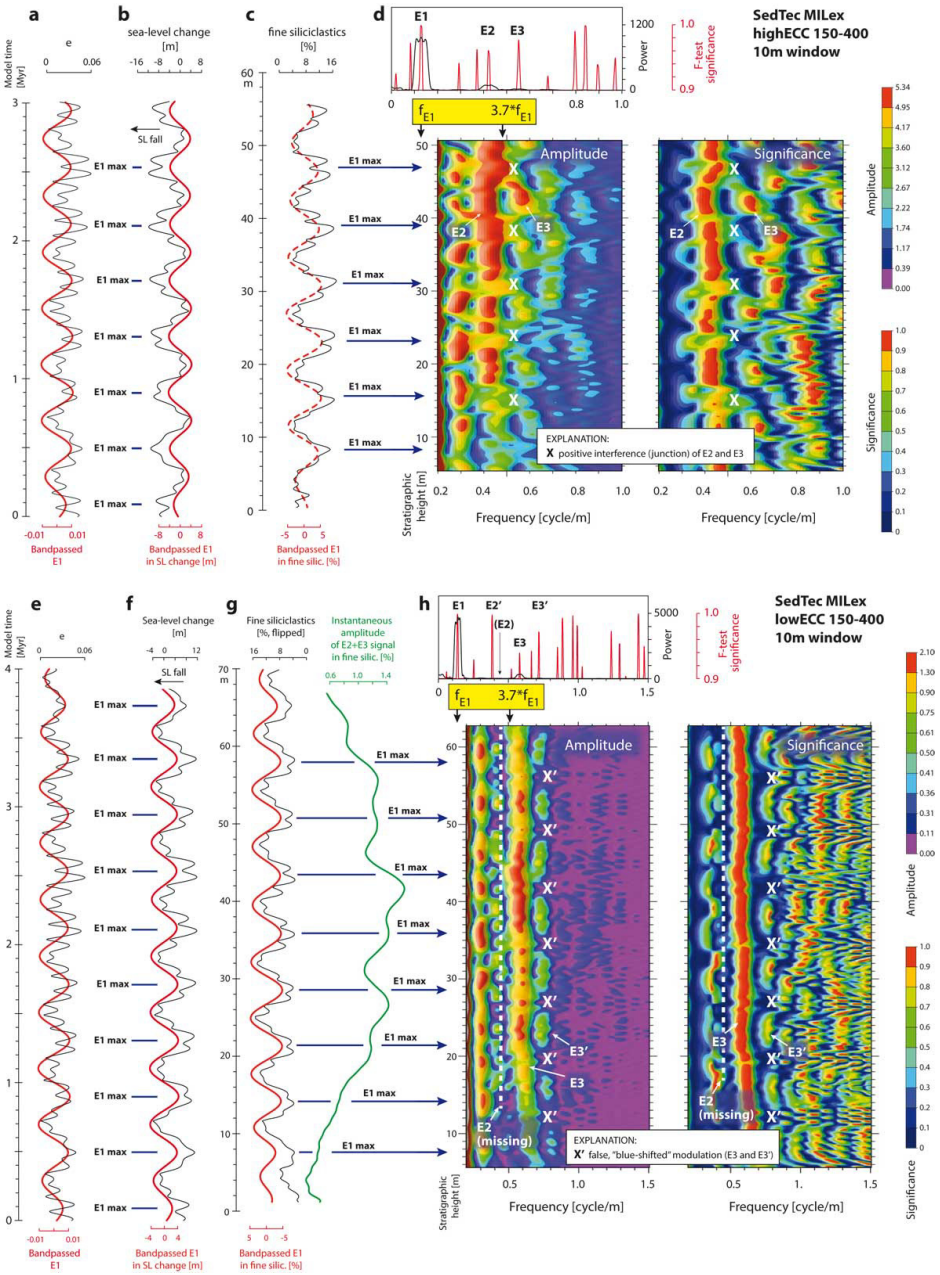

Figure S1.11. Examples of input and output parameters of two-dimensional models examining the effect of changing, sea-level controlled depositional topography on the preservation of AM and FM of orbital eccentricity (**models #29 and #32**; Table S2). **(a, e)** La2010d (93-97 Ma) solution for eccentricity (e) plotted against time. **(b, f)** Eccentricity-paced sea-level fluctuations calculated from the La2010d eccentricity (see Table S2 for details). **(c, g)** Selected model output: proportion of fine siliciclastics in dilution-driven hemipelagic strata. **(d, h)** Spectral estimates for the parameters shown in c and g: MTM (3 2π) power spectral and significance estimates for the entire series

(top), and EHA (MTM 3 2π) amplitude and significance obtained with a 10-m moving window. Frequencies corresponding to the eccentricity terms E1, E2 and E3, or theoretical positions of these frequencies (e.g., E2 in h), are indicated. E2' and E3' refer to distorted ("red" or "blue" shifted) frequencies of E2 and E3. Intervals of positive interference of the E2 and E3 signals are marked with X ("junctions"), while symbols X' refer to artificial modulations that form in the distorted signals. In these models, both X and X' modulations follow the same rhythm as the E1 signal. However, while the pristine interference patterns (X) trace closely the maxima in E1 eccentricity ("E1 max"), the artificial modulations (X' in h) are phase shifted relative to E1 maxima (the origin of this phase-lagged modulation is explained in Laurin et al. 2005). In this case, the key diagnostic feature of the distorted interference patterns is the "blue shift" of the modulated frequencies (~0.55-0.75 cycle/m in h): while the pristine interference features form between the frequencies E2 and E3, the distorted or "false" modulations form between E3 and E3' or between E2 and E2' (cf. Figures S1.7 through S1.10). The frequency band of the interfering components is therefore distinctly higher than the 3.7-th multiple of the recurrence frequency of the interference patterns (e.g., 3.7*0.14 = 0.52 cycle/m in h) observed in pristine FM (cf. Fig. 1).

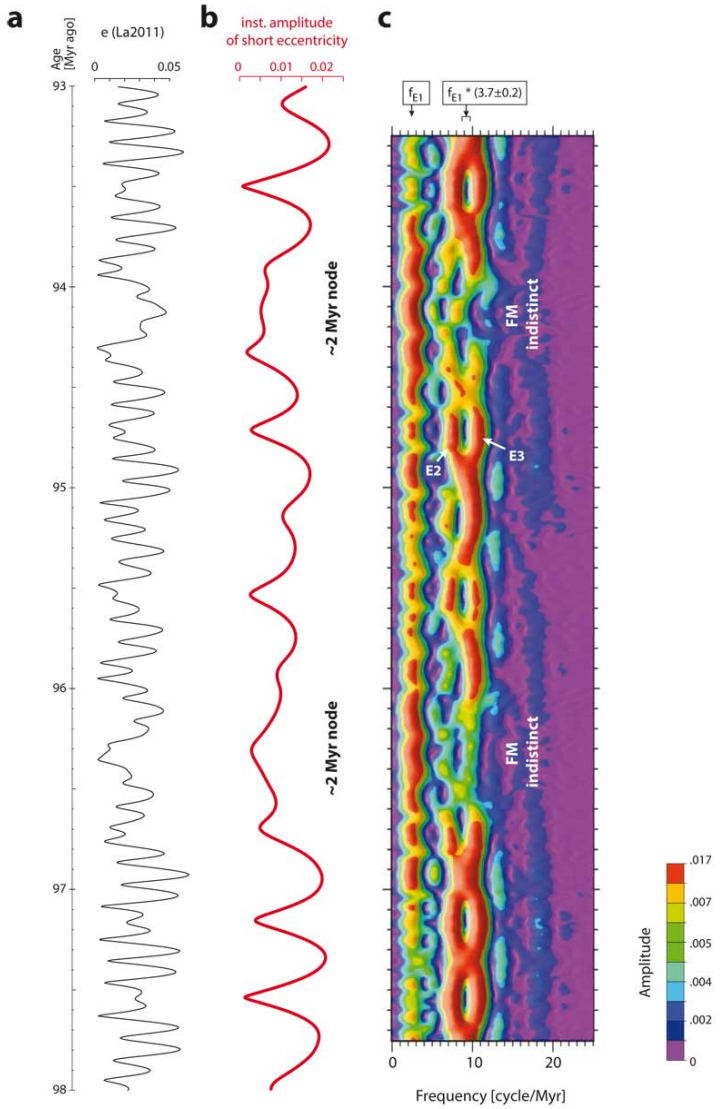

Figure S2
Inherent Myr-scale variability in the 405-kyr FM of E2 and E3. **(a)** Eccentricity solution La2011, interval 93-98 Myr ago (Laskar et al. 2011b). **(b)** Instantaneous amplitude of short eccentricity with ~2-Myr minima (nodes) indicated. **(c)** EHA amplitude spectrum for the bulk eccentricity (MTM 3 2p; 500 kyr window). Note that the interference of E2 and E3 terms is well developed only in intervals with relatively high amplitudes of short eccentricity. The Myr-scale nodes are marked by indistinct FM. This variability can be instrumental in interpreting the Myr-scale modulation in the deep past: Continuous series of well-defined FM patterns are unlikely to represent Myr-scale eccentricity minima, and can be interpreted as highs in the Myr-scale modulation. The opposite relationship (i.e., the use of indistinct FM to infer Myr-scale nodes) should not be routinely applied, because climatic and depositional processes involve a number of processes capable of distorting FM.

CASE STUDY: CENOMANIAN, Furlo

Spectral analysis of IRM data, Cenomanian, Furlo section
(data from Lanci et al. 2010).

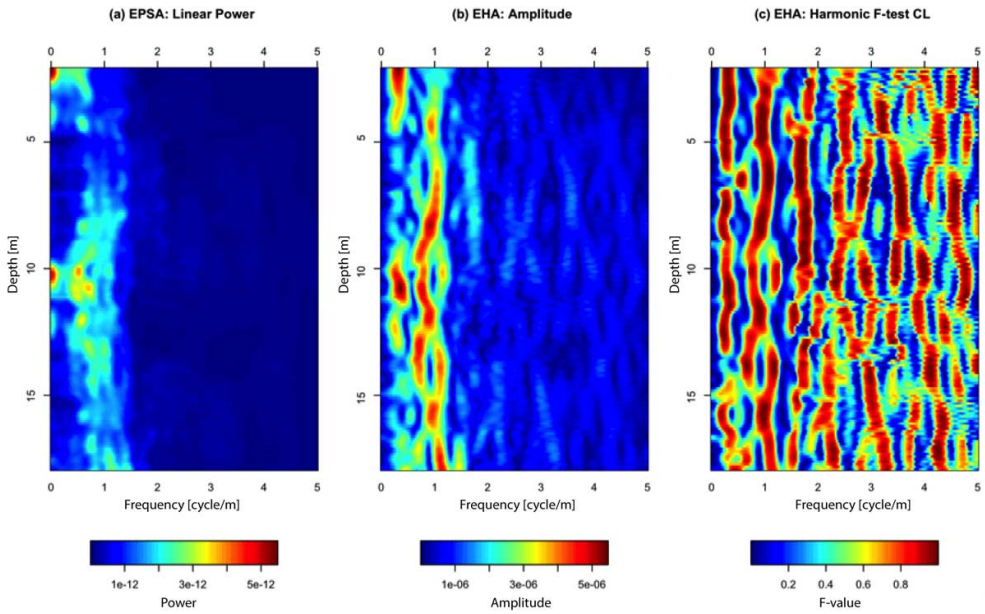

Figure S3.1
IRM data, Cenomanian, Furlo section. EHA (Evolutive Harmonic Analysis; Meyers et al. 2001) and EPSA (Evolutive Power Spectral Analysis; Meyers and Hinnov 2010) analyses conducted using a 4 m window, step 0.1 m, using 3 2π DPSS, and linear detrending. Median sampling interval is 8 cm. IRM data were interpolated to the sampling interval of 10 cm, using piecewise linear interpolation.

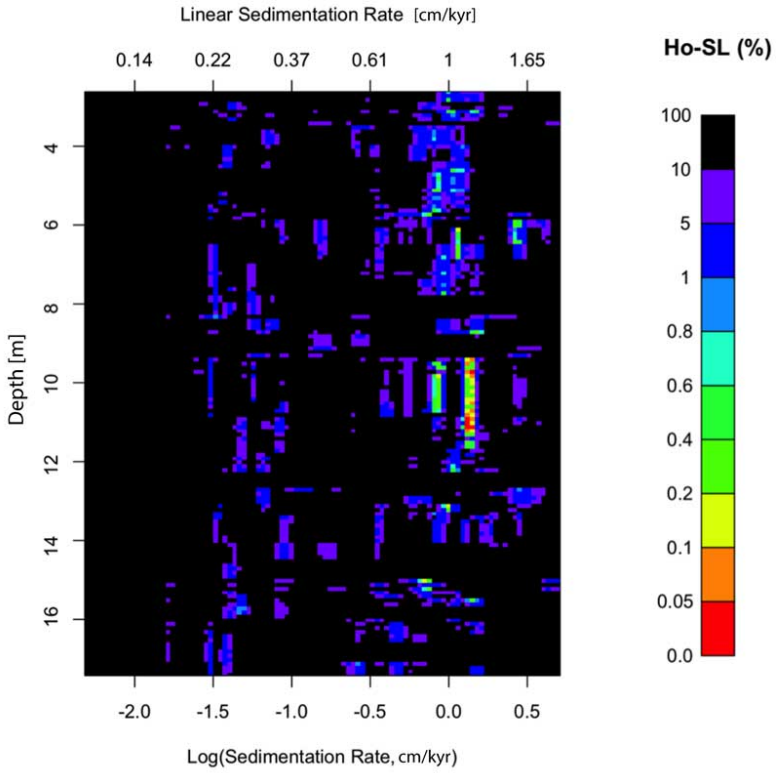

Figure S3.2
IRM data, Cenomanian, Furlo section. Evolutive Average Spectral Misfit (E-ASM) analysis of EHA spectral maxima exceeding the probability threshold of 0.8. EHA parameters: 5 m window, step 0.1 m, using 3 2π DPSS, and linear detrending. E-ASM parameters: Rayleigh = 0.1960784 cycles/m; Nyquist = 5 cycles/m; evaluating 100 sedimentation rates from 0.1-2 cm/kyr, with log-scaling for the grid; 100,000 Monte Carlo simulations; orbital target from Meyers et al. (2012b): 1/405.4739, 1/126.9841, 1/96.91096, 1/37.66478, 1/22.42152, 1/18.33181. Ho-SL: null hypothesis significance levels.

CASE STUDY: CENOMANIAN, Furlo

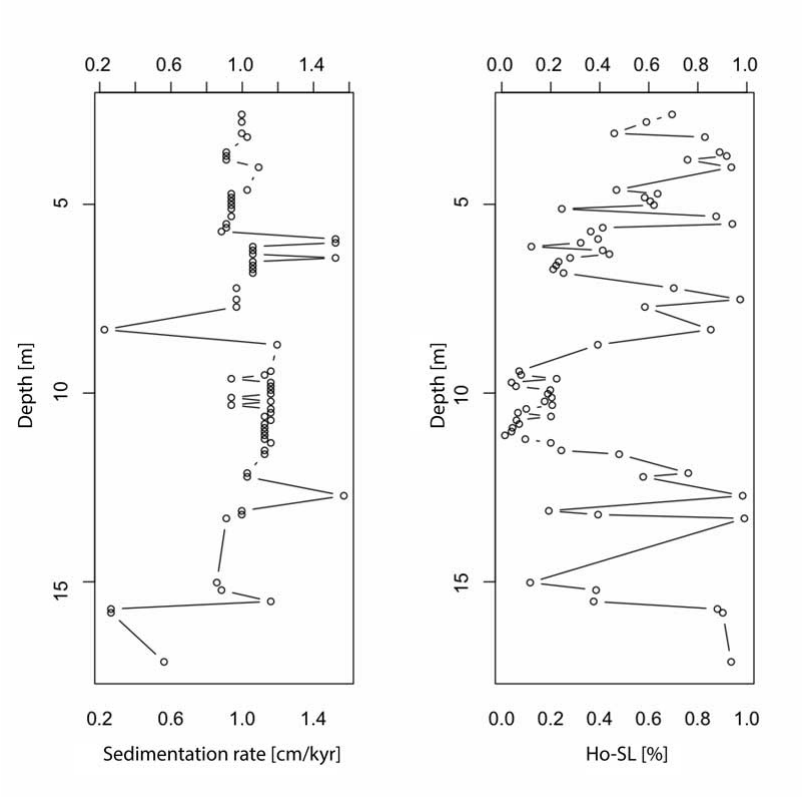

Figure S3.3
IRM data, Cenomanian, Furlo section. This plot illustrates all E-ASM results with null hypothesis significance levels <=1%. On the left are the resolved sedimentation rates, and on the right is the associated null hypothesis significance levels (Ho-SL). Notice the lowest Ho-SL levels centered on ~10 meters, and the stability of the resolved sedimentation rate through that interval.

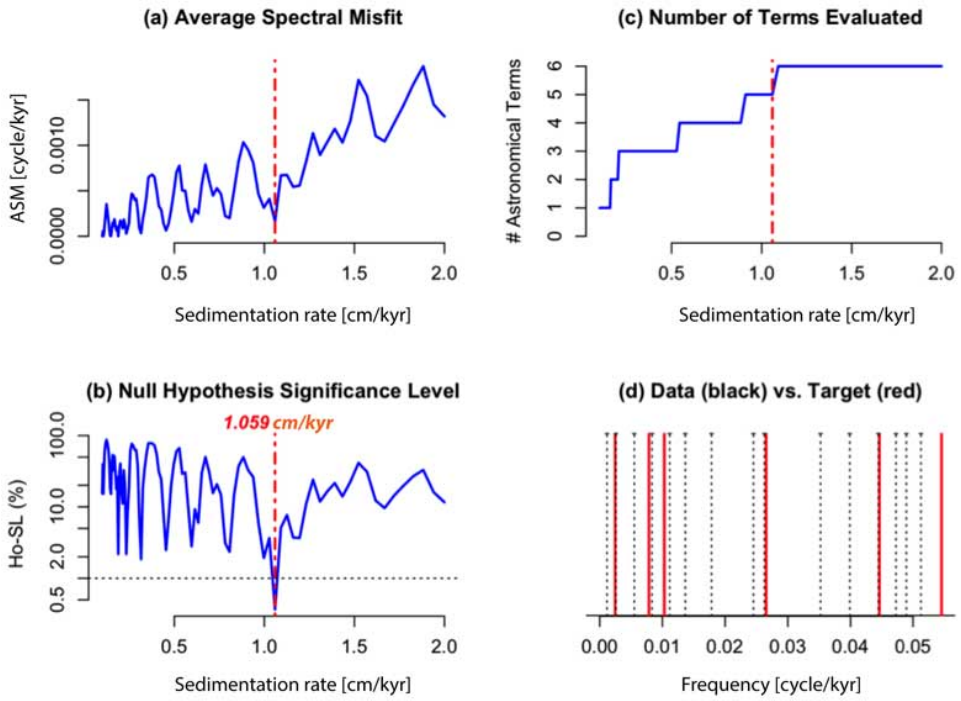

Figure S3.4
IRM data, Cenomanian, Furlo section. ASM (Average Spectral Misfit; Meyers and Sageman 2007) analysis for the entire interval using 3 2π DPSS. Probability Threshold = 0.9; Rayleigh = 0.05025126 cycles/m; Nyquist = 5 cycles/m; evaluating 100 sedimentation rates from 0.1-2 cm/kyr, with log-scaling for the grid; 100,000 Monte Carlo simulations. Orbital target from Meyers et al. (2012b): 1/405.4739, 1/126.9841, 1/96.91096, 1/37.66478, 1/22.42152, 1/18.33181

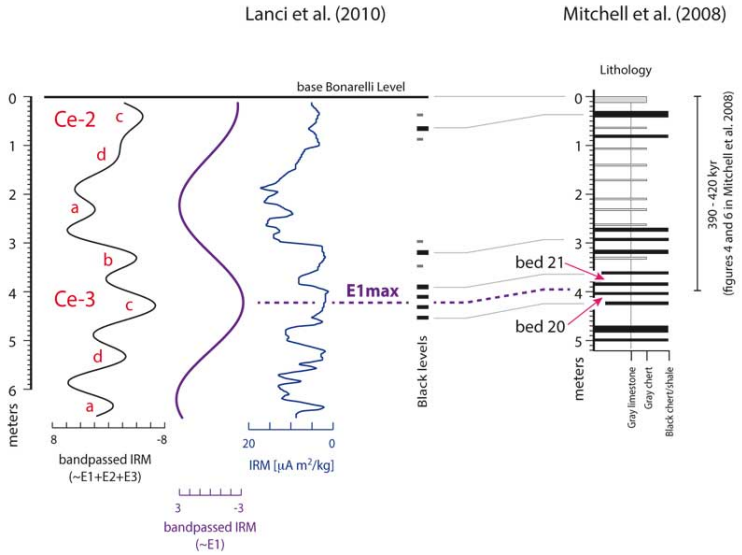

Figure S4.1.
Correlation of the astronomical age model from Mitchell et al. 2008 (right) with lithology and IRM from Lanci et al. 2010 (left), Furlo, Umbria-Marche Basin. Bandpassed eccentricity and the interpretation of 405-kyr eccentricity maximum (E1max) as in Figure 6 of this study. E1max is located between beds 20 and 21. According to Mitchell et al. (2008), the interval between the base of Bonarelli Level and interbed 20/21 spans 390 – 420 kyr.

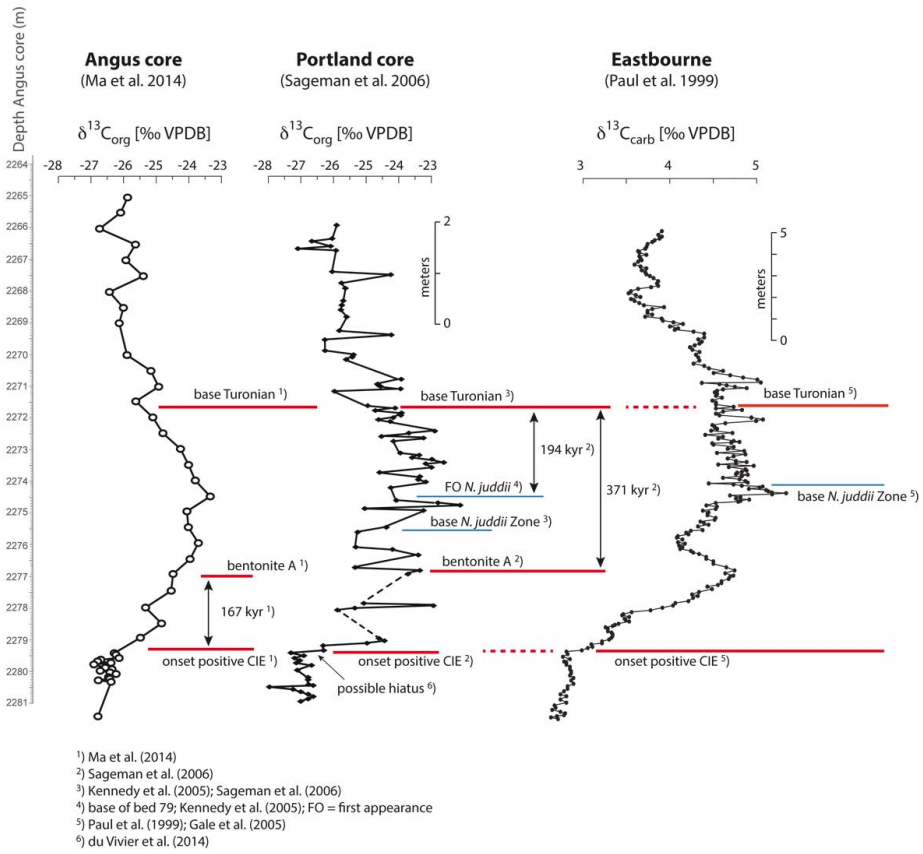

Figure S4.2. Construction of an age model for the OAE II interval. We use a combination of astrochronologies from Ma et al. (2014), which is well constrained in the lowermost part of OAEII, and that of Sageman et al. (2006), which is better constrained in the upper part of OAE II. Bentonite A provides a correlation marker connecting the Angus and Portland sections. This method suggests that the time span between the onset of positive CIE and the Cenomanian/Turonian boundary is 538 kyr (167 + 371 kyr). We estimate that the bulk uncertainty of the astrochronologies used in this calculation does not exceed two precessional cycles, i.e., ±20 kyr. The Eastbourne section was calibrated in the (floating) time domain using two age control points: (1) onset of positive CIE, and (2) base Turonian (C/T boundary in Fig. 6). The floating age was linearly interpolated between, and linearly extrapolated below and above these age control points.

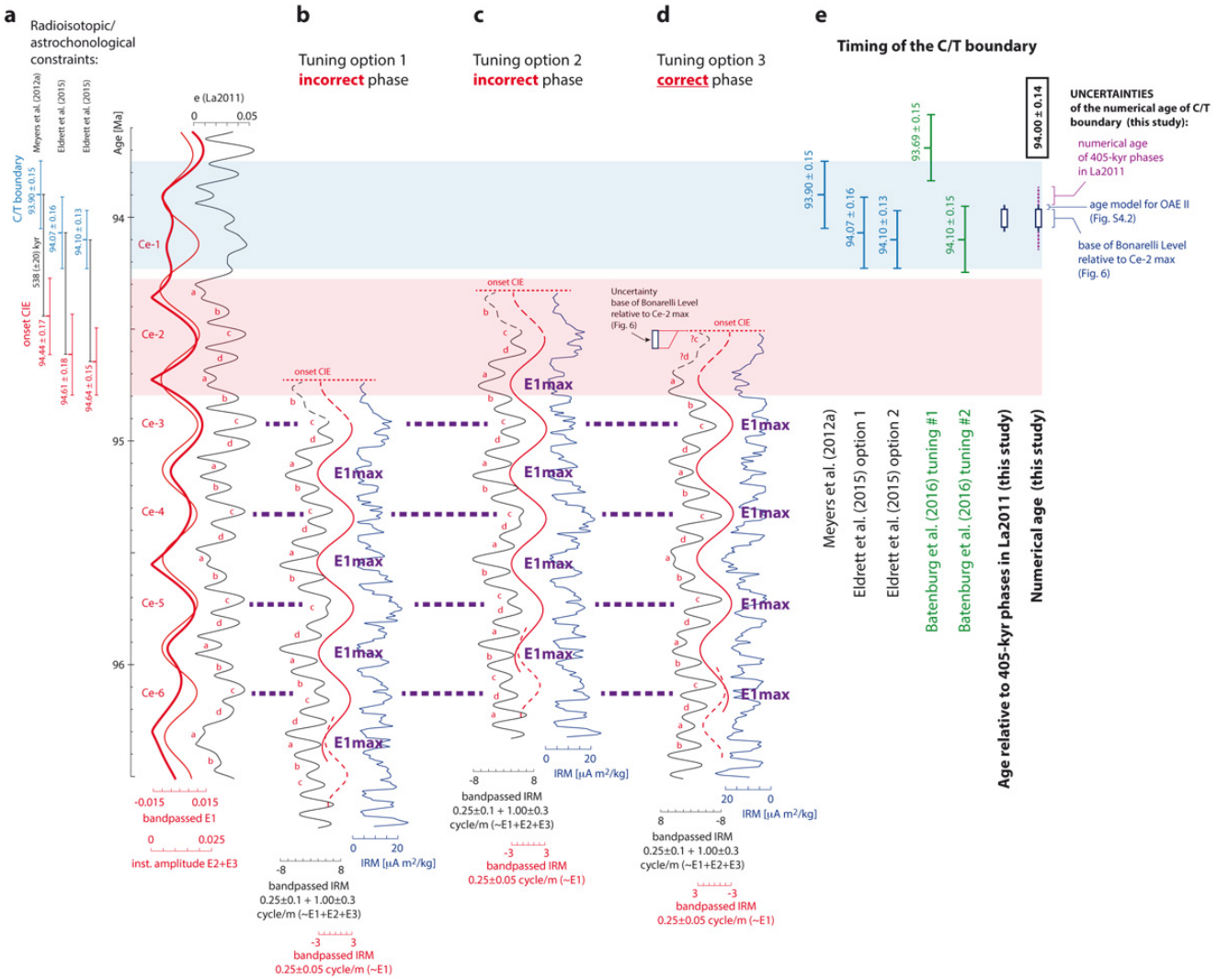

Figure S4.3. Options for correlating the Furlo eccentricity signature with the solution La2011. **(a)** La2011 solution (Laskar et al. 2011b): total eccentricity (black line), bandpassed 405-kyr term (2.5±0.5 cycle/Myr, Gaussian; thin red line) and instantaneous amplitude of short eccentricity (Hilbert transformed 9.5±2.5 cycle/Myr, Gaussian; thick red line). Maxima in E1 (405 kyr) eccentricity are labeled Ce-1 through Ce-6 and superimposed maxima in short eccentricity are labeled a through d. Ages of the Cenomanian-Turonian boundary (C/T; Meyers et al., 2012a; Eldrett et al. 2015) and the onset of positive carbon-isotope excursion (CIE; Fig. S4.2) are indicated. Blue and red bars indicate the range of age estimates for the C/T boundary and the onset of CIE, respectively. **(b-d)** Furlo section data: IRM (blue line; Lanci et al. 2010), sum of bandpassed eccentricity terms (E1+E2+E3; 0.25±0.10 + 1.00±0.30 cycle/m, Gaussian; black line), bandpassed 405-kyr term (0.25±0.05 cycle/m, Gaussian; red line). Furlo section data is plotted against stratigraphic depth (scale as in Fig. 6c). Note that three different correlation options are possible within the constraints of integrated (radiometric/astronomical) chronology. Options 1 and 2 are, however, incompatible with the location of interference patterns in the E2-E3 band that constrain the timing of E1 maxima and minima; E1max = 405-kyr maxima constrained by FM (Fig. 6c). **(e)** Age of the C/T boundary. The age estimate in our study is equipped with a total uncertainty of ±0.14 Myr, which is attributed to the uncertainties of (1) correlation of the base of

Bonarelli Level to the 405-kyr phases (±0.04 Myr; Fig. 6), (2) age model for the OAE II interval (±0.02 Myr; Fig. S4.2), and (3) numerical age of the 405-kyr phases in the solution La2011 (±0.08 Myr); this component is estimated from the maximum deviation in the timing of 405-kyr (2.5±0.5 cycle/Myr) maxima between 94 and 97 Myr ago in the solutions La2010a-d and La2011; the uncertainty estimate is compatible with the 0.16% maximum deviation in the 405-kyr period determined for the solutions La2010a-d by Laskar et al. (2011a). Note that our estimate of the C/T boundary age is compatible with the radiometric/astrochronological estimates of both Meyers et al. (2012a) and Eldrett et al. (2015). The confidence intervals associated with tuning #1 and #2 of Batenburg et al. (2016) overlap with the confidence interval of the radiometric/astrochronological estimate of Meyers et al. (2012a). Neither of the Batenburg et al. (2016) mean ages, however, overlap with the confidence interval of Meyers et al. (2012a), and the mean age of Meyers et al. (2012a) is not captured by the confidence intervals of tuning #1 or #2. Hence, following the rules for hypothesis testing (Smith 1997; Knezevic 2008) tuning options #1 and #2 of Batenburg et al. (2016) should be considered incompatible with the constraints in Meyers et al. (2012a). Similarly, tuning #1 of Batenburg et al. (2016) is incompatible with the age estimates in Eldrett et al. (2015).

CASE STUDY: EOCENE, Contessa

Spectral analysis of $CaCO_3$ data, Eocene, Contessa Road section
(data from Galeotti et al. 2010).

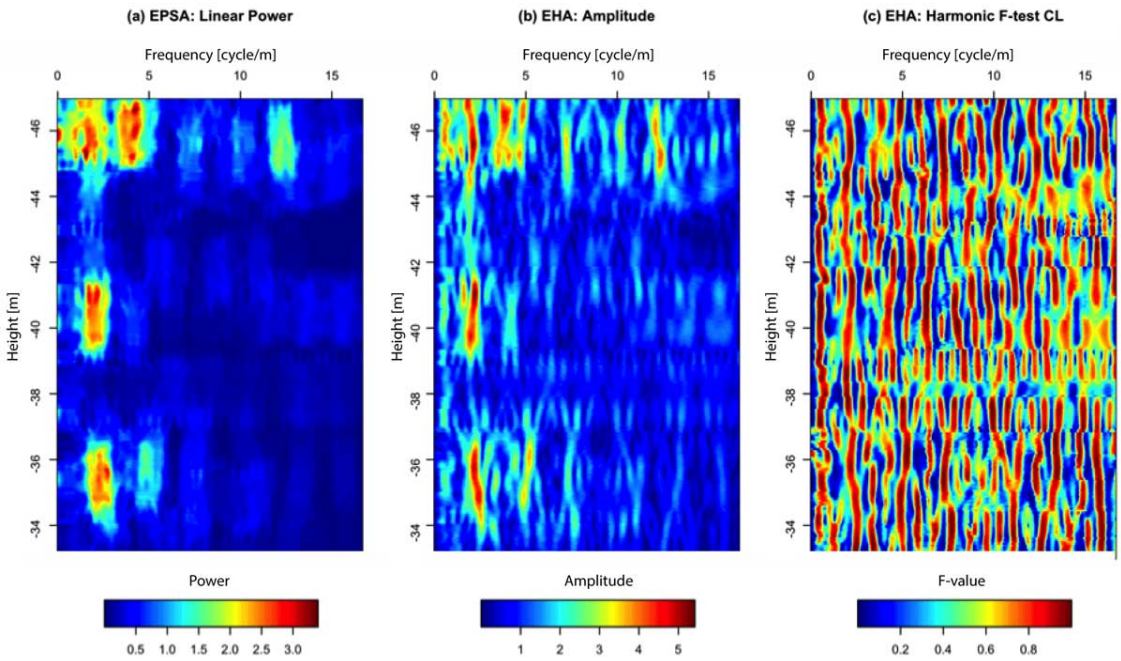

Figure S5.1
$CaCO_3$ data, Eocene, Contessa Road section. EHA (Evolutive Harmonic Analysis; Meyers et al. 2001) and EPSA (Evolutive Power Spectral Analysis; Meyers and Hinnov 2010) analyses conducted using a 2.49 m window, step 0.06 m, using 3 2π DPSS, and linear detrending. Wt.% $CaCO_3$ data were interpolated to the median sampling interval of 3 cm, using piecewise linear interpolation.

CASE STUDY: EOCENE, Contessa

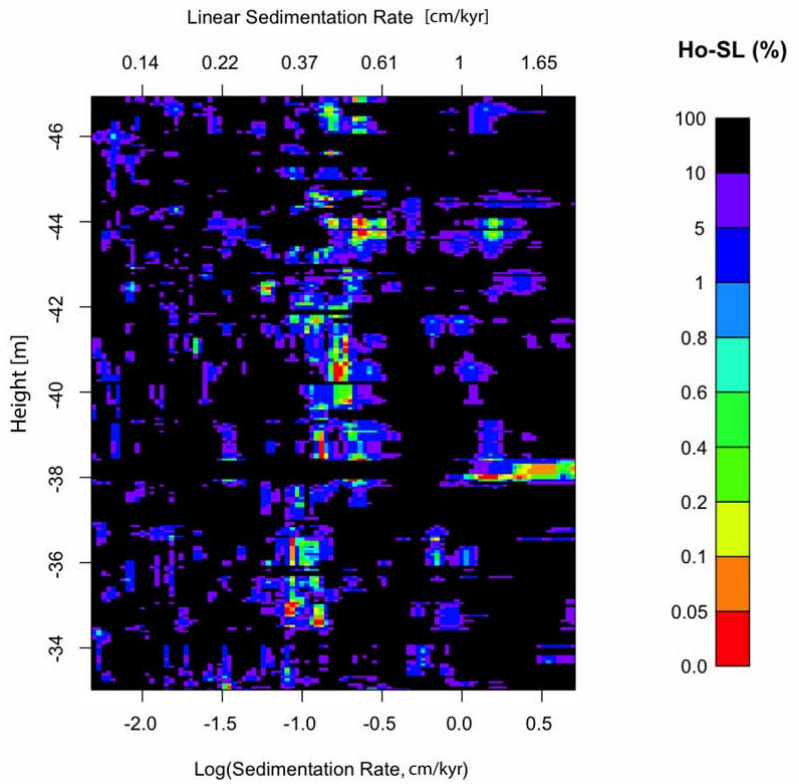

Figure S5.2
$CaCO_3$ data, Eocene, Contessa Road section. Evolutive Average Spectral Misfit (E-ASM) analysis of EHA spectral maxima exceeding the probability threshold of 0.8. EHA parameters: 2.49 m window, 3 2π DPSS. E-ASM parameters: Rayleigh = 0.3968254 cycles/m; Nyquist = 16.66667 cycles/m; evaluating 100 sedimentation rates from 0.1-2 cm/kyr, with log-scaling for the grid; 100,000 Monte Carlo simulations; orbital target estimated from Laskar et al. (2004) solution (Meyers et al. 2012b): 1/405.6795, 1/123.839, 1/94.87666, 1/50.59022, 1/39.26702, 1/23.04147, 1/21.81818, 1/18.56436

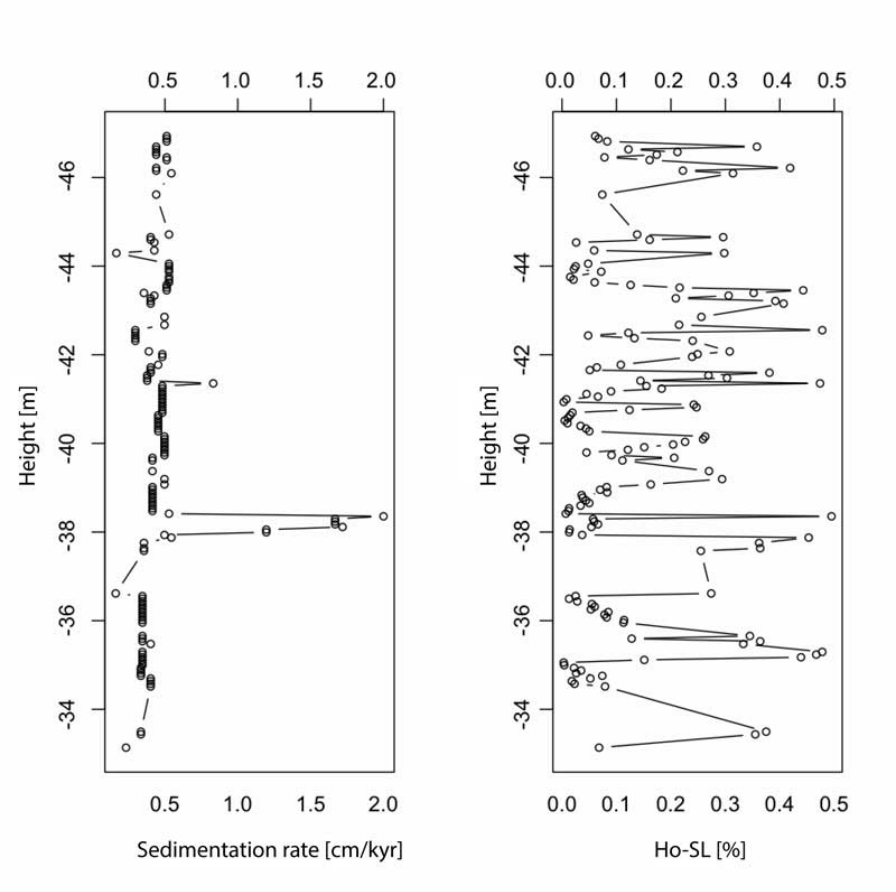

Figure S5.3
$CaCO_3$ data, Eocene, Contessa Road section. This plot illustrates all E-ASM results with null hypothesis significance levels <=0.5%. On the left are the resolved sedimentation rates, and on the right are the associated null hypothesis significance levels (Ho-SL). The high sedimentation rate at approximately -38 m coincides with a node in the long-term eccentricity cycle (see Fig. 7), and can be an artifact of the loss of signal. Otherwise, the E-ASM sedimentation rate result is remarkably stable.

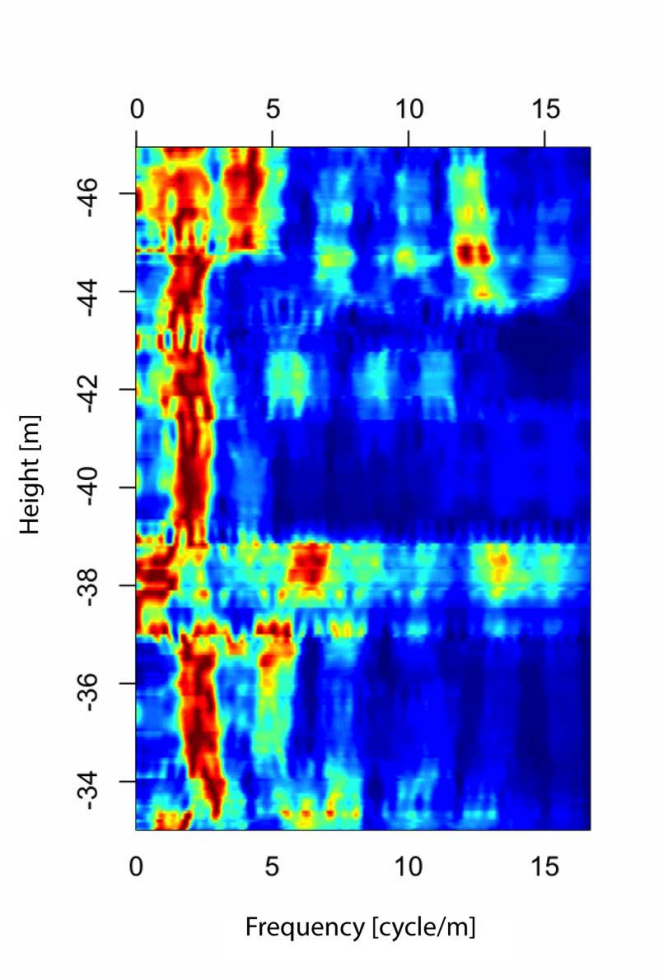

Figure S5.4
$CaCO_3$ data, Eocene, Contessa Road section. The 2.49 m EPSA results (Fig. S5.1) have been normalized such that each window has a maximum power of 1. This further illustrates the remarkable stability of the identified short eccentricity term (except of the short interval at approximately -38 m).

REFERENCES

(cited in SI only)

Gale AS, Kennedy WJ, Voigt S, Walaszczyk I (2005) Stratigraphy of the Upper Cenomanian–Lower Turonian Chalk succession at Eastbourne, Sussex, UK: Ammonites, inoceramid bivalves and stable carbon isotopes. *Cretaceous Res.* 26: 460–487, doi:10.1016/j.cretres.2005.01.006.

Kennedy WJ, Walaszczyk I, Cobban WA (2005) The Global Boundary Stratotype Section and Point for the base of the Turonian Stage of the Cretaceous: Pueblo, Colorado, U.S.A. *Episodes* 28(2): 93-104.

Knezevic A (2008) Overlapping Confidence Intervals and Statistical Significance, *StatNews* 73, Cornell Statistical Consulting Unit. https://www.cscu.cornell.edu/news/statnews/stnews73.pdf

Ma C, Meyers SR, Sageman BB, Singer BS, Jicha BR (2014) Testing the astronomical time scale for oceanic anoxic event 2, and its extension into Cenomanian strata of the Western Interior Basin (USA). *Geol. Soc. Am. Bul.* 126: 974-989.

Meyers SR, Hinnov LA (2010) Northern Hemisphere glaciation and the evolution of Plio-Pleistocene climate noise. *Paleoceanography* 25: PA3207.

Sageman BB, Meyers SR, Arthur MA (2006) Orbital time scale and new C-isotope record for Cenomanian-Turonian boundary stratotype. *Geology* 34: 125-125.

Smith RW (1997) Visual hypothesis testing with confidence intervals. *Proceedings of the Twenty-Second Annual SAS Users Group International Conference* (SUGI 22). http://www2.sas.com/proceedings/sugi22/STATS/PAPER270.pdf